K-SHELL IONIZATION CROSS SECTIONS FOR ELEMENTS SE TO PD: 0.4 to 2.0 MeV

DISSERTATION

Presented to the Graduate Council of the
North Texas State University in Partial
Fulfillment of the Requirements

For the Degree of

DOCTOR OF PHILOSOPHY

By

Tommy L. Criswell
Denton, Texas

December, 1974

Criswell, Tommy Lemuel, K-Shell Ionization Cross Sections for Elements Se to Pd: 0.4 to 2.0 MeV. Doctor of Philosophy (Physics), December, 1974, 58 pp. 4 tables, 7 illustrations, appendix, bibliography, 94 titles.

K-Shell ionization cross section for protons over the energy range of 0.4 to 2.0 MeV have been measured on thin targets of the elements Se, Br, Rb, Sr, Y, Mo and Pd. Total x-ray and ionization cross sections for the K-shell are reported. The experimental values of the ionization cross sections are compared to the non-relativistic plane-wave Born approximation, the binary-encounter approximation, the constrained binary-encounter approximation, and the plane-wave Born approximation with corrections for Coulomb-deflection and binding energy effects.

PLEASE NOTE:

Pages iv-vi are lacking in number only. Not available for microfilming.

UNIVERSITY MICROFILMS.

TABLE OF CONTENTS

LIST OF TABLES

LIST OF ILLUSTRATIONS

CHAPTER I

INTRODUCTION

With the development of the high-resolution Si(Li) detector by Elab and Nakamura,[1] technological applications of inner-shell ionization by heavy particle bombardment appeared feasible.[2,3] For example, in trace element analysis of semiconductors, concentrations of 10^{-13} atomic per cent could be detected[4] in a Si substrate. However, a major obstacle to developing accurate analytical techniques was the ±30% experimental error of the existing ionization cross section data.[5] Recent, more accurate measurements of ionization cross sections using thin targets have been reported and are reviewed through April, 1973,by Rutledge and Watson.[6] The number of elements studied in this manner is small and those elements have been investigated at only a few, widely spaced bombarding energies. In order to provide the necessary data on inner-shell ionization by light ions over an energy range generally accessible to the large number of industrial and public laboratories equiped with Van de Graaff accelerators, studies have been made at North Texas State University using protons with energies from 0.4 to 2.0 MeV on the elements Fe to As[7,8] Se to Pd,[9,10] Ag to La,[11,12] Pr to Dy,[13,14,15] and Ho to Bi.[16-20]

Thin transmission-mounted targets were used in order to minimize beam energy degradation and self-absorption in the target. A Si(Li) spectrometer detected the x rays. The data were compared to extant theories and independent data.

This dissertation is based on one of the above studies.[9] The specific elements studied were Se, Br, Rb, Sr, Y, Mo, and Pd. The incident protons had energies from 0.4 to 2.0 MeV. The data were compared to the plane-wave Born approximation,[21] the corrected plane-wave Born approximation,[22] the binary encounter approximation,[23] the constrained binary encounter approximation,[24] and the relativistic plane-wave Born approximation.[25] Reasonably good agreement was found between the present data and the data of Bearse, et al.,[26] Duggan, et al.,[27] and Ferree.[28] The x-ray cross sections for Br, Sr, and Y have not previously been measured. The cross section for Mo has not been measured using thin targets.

Although interest in the applications of heavy-ion-induced ionization developed only recently, this process has been studied since 1912. Following the observation by Gray[29] that elements irradiated by beta rays from radium emit x rays, Chadwick[30] demonstrated that the more massive alpha particles also emitted by radium were able to excite x rays in various target materials. Subsequent measurements by Chadwick and Russell[31] revealed the x rays to be the characteristic x rays of the target element. Thus the x rays were the result of inner-shell ionization due to the alpha-particle bombardment. Thompson[32] found that x rays

were produced when positive ions accelerated through only a 1000-V potential struck thick targets. Slater[33] identified the K- and L-shell x rays of tin and lead under alpha-particle bombardment. Noting that even very low-velocity ions could produce x rays, Gerthsen[34] pointed out that in order for sufficient energy to be transferred to the bound electrons by the slow incident ions, the velocity of the bound electrons must be considered.

Bothe and Franz[35] used the alpha particles from polonium to obtain excitation functions for the K-, L-, and M-shell x rays for the elements Z=12 to 30, Z=34 to 79, and Z=83, respectively. Using a Geiger counter and alpha particles with energies up to 5.1 MeV, Bothe and Franz found the absolute cross section for aluminum and relative cross sections for the remaining elements. The cross sections were found to decrease with increasing Z of the target element and increase with bombarding energy.

Barton[36] attempted the first study of x-ray production from proton bombardment. He accelerated protons to 25 keV, but was unable to detect any resulting x rays. Gerthsen and Reusse[37], using 30 to 150 keV protons and Geiger counters, observed the K-shell x rays of Al and Mg and the L-shell x rays of Se. Relative excitation functions were measured. Peter[38] later added an absolute cross section measurement for 132-keV protons on Al. Gerthsen's results had the same atomic number and bombarding energy dependences as Bothe's.

Henneberg[39] successfully applied the non-relativistic

plane-wave Born approximation to K-shell ionization by protons and alphas. The theory agreed well qualitatively with the relative excitation functions given by Bothe[35] and by Gerthsen.[37] However, the bombarding energy range was small and the experimental errors were large. The more careful relative cross section measurements by Peter[38] for protons between 60 and 170 keV duplicated Gerthsen's work,[37] but also were restricted in bombarding energy range.

Livingston, Genevese, and Konopinski[40] used a cyclotron to obtain proton energies of up to 1.76 MeV to study x-ray production in targets from Z=12 to 82. Their measurements, made with an ionization chamber, were in qualitative agreement with Henneberg's theory. Cork[41] bombarded thirty-eight elements with deuterons from a cyclotron with energies to 10 MeV. Since photographic plates were used as detectors, the interpretation of the data was limited to the conclusion that the x-ray production cross section increases with increasing energy and decreases with increasing Z.

Simane and Urbanec[42] used a high-resolution Bragg spectrometer to study the relative excitation functions for x-ray production by 400 to 700 keV protons on Z=26 to 30. They reported agreement with the theory of Henneberg.[39]

The advent of the sodium iodide scintillation counter enabled researchers to measure absolute x-ray production cross sections. Lewis, Simmons, and Merzbacher[43] studied the K-shell x rays from thick targets of Mo, Ag, Ta, Au, and Pb from 1.7 to 3.0 MeV proton bombardment. Bevington

and Bernstein[44] studied Ti, Fe, and U over a similar energy range. Bernstein and Lewis[45] studied the L-shell of Ta, Au, Pb, and U, using protons with energies between 1.5 and 4.25 MeV. Zupancic and Huus[46] reported x-ray production cross sections for Sn due to incident protons. Hansteen and Messelt[47] reported ionization cross sections for the K-shell of Cu and Mo, using protons with energies between 0.2 and 1.6 MeV. Using a proportional counter, Singh[48] studied the K-shell ionization of Cu and Ag for incident protons, deuterons, and alphas with energies between 0.4 and 1.0 MeV. Using a Na(I) detector, Messelt[49] reported K-shell ionization cross sections for Fe, Cu, Mo, Ag, Sn, and Ta under proton bombardment with energies between 0.14 and 1.3 MeV. Jopsen et al.[50] reported ionization cross sections for twenty-six elements from Z=22 to 92 for 0.10 to 0.50 MeV protons. Khan et al.[51-58] using proportional counters, studied numerous elements from carbon to holmium with 0.10 to 1.90 MeV protons. Numerous investigators have used proportional counters to study elements from carbon to uranium over an energy range from 0.015 to 28.0 MeV. Reviews of measured cross sections have been made by Garcia et al.,[5] and Rutledge and Watson.[6]

Jamnik and Zupančič[25] reevaluated the plane-wave Born approximation (PWBA) for K-shell ionization by protons and alphas in terms of relativistic hydrogenic wave functions. Ionization cross section values were given for Pb and Ag[59] at several bombarding energies. These values were compared to the recent work of Lewis[43] and found to improve the agreement

between theory and experiment. However, discrepancies were found in the energy dependence of the theory, as compared to the measured values. The authors noted that deflection of the incident particle in the field of the target nucleus should be included in a more complete treatment, and speculated that such a correction would improve the agreement with the energy dependence of the data.

Merzbacher and Lewis[21] presented a more complete treatment of the non-relativistic PWBA that does not involve some of the approximations Henneberg[39] used. The PWBA tends to be too high with respect to the data over most of the proton (or alpha) energy range, with the greatest disparity occurring as the incident particle velocity approaches the average velocity of the K-shell electrons. But complications exist in the interpretation of experimental results at the high energies. Even at low energies, when an electron is ejected by collision with the incident particle, an Auger electron may be emitted, rather than the corresponding x ray. Thus, the theoretical ionization cross section must be related to the measured x-ray production cross section by the fluorescence yield ω_K, the ratio of the number of x rays emitted to the number of ionizations. The values for ω_K taken from the literature[60] may not be well established. This difficulty is compounded as the bombarding energy increases. The probability for multiple ionization of the atom increases,[61] and the fluorescence yield may be caused to vary appreciably.[62]

Data interpretation is also complicated by the resolving power of the Na(I) detector and proportional counter. Since the peaks of the pulse-height spectra are rather broad, the peak-to-background ratio is relatively small. Thick targets must then be used so that the maximum x-ray yield is obtained. X rays are being produced by protons with all energies between the incident energy and zero. One obtains the integrated yield for all energies. In terms of the range of the particle in the target, the yield may be written as

where R is the distance into the target, $\sigma_X(E(R))$ is the x-ray production cross section, R_0 is the particle range, n is the number of target atoms per unit volume, E is the particle energy, and μ is the average absorption coefficient. By differentiation of Eq. (1.1) one obtains

The difficulties arise in measuring the slope of the yield curve, determining the values of μ, and establishing the values of the stopping powers dE/dR. Basbas *et al.*[22] quote a lower limit of the experimental error due to these effects to be 30 per cent.

With the development of the Si(Li) detector,[1] detector

resolution was improved by a factor of ten, with a corresponding increase in the peak-to-background ratio. This improvement allowed researchers both to study many of the individual subshell transitions and to use thin targets. This procedure was first used by Richard[63] to measure the absolute cross sections for Cu ionization due to proton and oxygen bombardment. Rutledge and Watson[32] have reviewed the numerous studies made through the spring of 1973. Earlier reviews were made by Lin et al.,[64] and Garcia et al.[5] Current studies that incorporate Si(Li) detectors and thin targets report total experimental errors of 10 per cent and reproducibility of 2 per cent under favorable conditions.

Concurrent with these improvements in experimental accuracy, Basbas, Brandt, and Laubert[22] incorporated refinements in the PWBA. Using the correction for the Coulomb deflection of the incident particle by the target nucleus as given by Bang and Hansteen,[65] and correcting for the increase in atomic binding due to the penetration of the K-shell by the projectile, Brandt et al.[22] improved the agreement with experiment over much of the energy range (see Chap IV.).

Noting the equivalence of the quantal and classical two-body Rutherford cross section, Garcia[23] applied Gryzinski's[67] classical description of an incident particle scattering from a bound particle to the case of proton-induced ionization of the K-shell. Because only the motions of the bound and incident particles enter the theory, the formulation is called

the binary encounter approximation (BEA). The principal advantages of this classical theory are its simplicity and relatively good agreement with data over large ranges of the bombarding energy. A recent refinement of the BEA by Hansen[24] uses hydrogenic momentum-space wave functions to obtain the necessary velocity distribution of the bound electrons.

The PWBA, BEA, Brandt et al.[22] corrections to the PWBA, Hansen's[24] BEA, and relativistic PWBA (PWBAR) are outlined in Chapter II. The experimental procedure is discussed in Chapter III, and the experimental results are compared to theory and independent experiments in Chapter IV. The PWBAR is treated in more detail in the Appendix.

CHAPTER II

THEORY OF ATOM-ION COLLISIONS

The impact between a fast proton and a bound electron would appear to be adequately described only by quantum mechanics. Yet the successes of the classical BEA in fitting the experimental data seem to contradict this assumption. In this section, we will describe these two theories, and make modifications to their most elementary forms. We begin with the PWBA of Merzbacher[21] as the basic quantum mechanical theory. This discussion will be followed by the BEA theories of Garcia[5] and Hansen[24], and then a description of the Coulomb deflection and binding energy corrections as they apply to the PWBA. The remainder of this section will then be devoted to the relativistic PWBA.[25]

The Plane-Wave Born Approximation

The plane-wave Born approximation calculation due to Merzbacher[21] assumes that the incident particle is described as a plane wave, a small amplitude of which is scattered by the target atom. Following the development of Mott and Massey,[67] we look then for proton wave functions given by

$$F \propto e^{ikz} + \frac{1}{r} e^{ikr} f(\theta,\phi), \qquad (2.1)$$

where z is the axis of incidence, and $f(\theta,\phi)$ is the usual scattering amplitude. The solution of Schrödinger's equation for the full ion-atom system will yield $f(\theta,\phi)$, and any restrictions on the validity of the plane-wave approximation will be obtained.

The wave equation for the ion-atom system is

$$\left[\frac{\hbar^2}{2m_1}\nabla_1^2+\frac{\hbar^2}{2m_2}\nabla_2^2+E-\frac{Z_1Ze^2}{r_1}+\frac{Ze^2}{r_2}+\frac{Z_1e^2}{r_{12}}\right]\Psi=0 \qquad (2.2)$$

The incident ion is denoted by the subscript 1, the target atom electron by subscript 2. E is the sum of the electron binding energy and the ion kinetic energy, and Z the atomic number of the atom. The origin for the coordinates $\vec{r}_1$ and $\vec{r}_2$ is the nucleus of the target atom. The Hamiltonian does not include a term involving the motion of the nucleus. This term may be omitted because protons incident on targets of mass of about 100 a.m.u. will cause the nucleus to recoil only slightly.

To proceed, some assumptions must be made about the form of the wave function. Mott[68] has argued that, if the charge of the projectile is small compared to the target atomic number and not large compared to the electron charge, the electronic states will not be greatly distorted from their undisturbed configuration. The total wave function may then be written as the product of the atomic (ψ_n) and projectile (F_n) wave functions,

$$\Psi = \psi_n(\vec{r}_2)\, F_n(\vec{r}_1)\,, \qquad (2.3)$$

where $\psi_n(\vec{r}_2)$ is chosen to be the normalized hydrogenic wave function of energy E_n satisfying

$$\left(\frac{\hbar^2}{2m_2}\nabla_2^2 + E_n + \frac{Ze^2}{r_2}\right)\psi_n(\vec{r}_2) = 0 \quad . \qquad (2.4)$$

Eq. (2.4) then becomes

$$\left(\frac{\hbar^2}{2m_2}\nabla_2^2 + E_n + \frac{Ze^2}{r_2}\right)\psi_n(\vec{r}_2)F_n(\vec{r}_1) \qquad (2.5)$$

$$+\left(\frac{\hbar^2}{2m_1}\nabla_1^2 + E - E_n + \frac{Z_1e^2}{r_{12}} - \frac{Z_1Ze^2}{r_1}\right)\psi_n(\vec{r}_2)F_n(\vec{r}_1) = 0.$$

The first term is zero from Eq. (2.4). If Eq.(2.5) is multiplied by $\psi_n^*(\vec{r}_2)$ from the left and integrated over $\vec{r}_2$, we obtain

$$\left(\frac{\hbar^2}{2m_1}\nabla_1^2 + E - E_n\right)F_n(\vec{r}_1) = \int\left(\frac{Z_1e^2}{r_{12}} - \frac{Z_1Ze^2}{r_1}\right)\psi_n F_n\, d\vec{r}_2\,. \qquad (2.6)$$

The plane-wave description of the incident projectile may be regained from Eq. (2.6) by letting $\vec{r}_1$ be very large. The integral on the right is then zero and $F_n(\vec{r}_1)$ satisfies

$$\left[\nabla_1^2 + \frac{2m_1}{\hbar^2}(E - E_n)\right]F_n(\vec{r}_1) = 0\,, \qquad (2.7)$$

which is the equation for a plane wave.

The incident plane wave is the representation of the

actual, collimated proton beam. In practice this collimation does not allow the unscattered beam to enter the detector. Thus the scattered beam is described by the term $r^{-1} \exp(ik_n r) \cdot f_n(\theta,\phi)$ in Eq. (2.1). At a distance r from the scatterer the probability of finding a particle that has populated the state n is given by[69]

$$\sigma_n(\theta,\phi)\, d\Omega = \frac{2\pi}{\hbar} \frac{\rho\, |f_n(\theta,\phi)|^2}{v_1 L^{-3}}, \qquad (2.8)$$

where ρ is the density of final states, v_1/L^3 is the incident flux, $r^{-2} \left| f_n(\theta,\phi) \right|^2$ is the number of projectiles per L^3 at the position $\vec{r}$, and L^3 is the unit volume of normalization for the incident plane wave. The density of states is

$$\frac{m_1^2 L^3 v_1' \, d\Omega}{8\pi^3 \hbar^3}, \qquad (2.9)$$

where v_1' is the velocity of the outgoing proton, and $d\Omega$ is the solid angle into which the proton is scattered. Thus the scattering cross section is

$$\sigma_n = \frac{v_1'}{v_1} \frac{m_1^2 L^6}{4\pi^2 \hbar^2} |f_n(\theta,\phi)|^2. \qquad (2.10)$$

The incident and scattered plane waves are box normalized; so the term $f_n(\theta,\phi)$ is proportional to L^{-3}. The cross section therefore does not depend on the size of the normalization volume.

From Eq. (2.1), the expression for $f_n(\theta,\phi)$ is given by

the solution of the inhomogeneous equation

$$\left(\frac{\hbar^2}{2m_1}\nabla_1^2 + E - E_n\right)F_n(\vec{r}_1) = \int \psi_n^*\left(\frac{z_1e^2}{r_{12}} - \frac{z_1 z e^2}{r_1}\right)\Psi\, d\vec{r}_2. \quad (2.11)$$

In the first Born approximation, the function Ψ is replaced with the initial, undisturbed functions of the projectile and the ground state atom,

$$\Psi = \exp(ik_0\hat{r}_0\cdot\vec{r}_1)\,\psi_0(\vec{r}_2). \quad (2.12)$$

Substitution of the expression for Ψ into Eq. (2.12) gives

$$\left(\frac{\hbar^2}{2m_1}\nabla_1^2 + E - E_n\right)F_n(\vec{r}_1)$$

$$= \int \psi_n^*\left(\frac{z_1e^2}{r_{12}} - \frac{z_1 z e^2}{r_1}\right)\exp(ik_0\hat{r}_0\cdot\vec{r}_1)\,\psi_0(\vec{r}_2)\, d\vec{r}_2. \quad (2.13)$$

Knowing the homogeneous solution for $F_n(\vec{r}_1)$ from Eq. (2.7), we may use the Green's function method of solution[70] to solve Eq. (2.13) for $F_n(\vec{r}_1)$, yielding

$$F_n(r) = \frac{m_1}{2\pi\hbar^2}\iint \frac{\exp(ik_n|\vec{r}-\vec{r}_1|)}{|\vec{r}_1-\vec{r}|}\exp(ik_0\hat{r}_0\cdot\vec{r}_1)$$

$$\times\left(\frac{z_1 z e^2}{r_1} - \frac{z_1 e^2}{r_{12}}\right)\psi_0(\vec{r}_2)\,\psi_n^*(\vec{r}_1)\, d\vec{r}_1\, d\vec{r}_2. \quad (2.14)$$

The radius r at which the scattered particle is detected is at a laboratory distance from the scattering center (i.e., $|\vec{r}| \gg |\vec{r}_1-\vec{r}_2|$). An expansion of $|\vec{r}_1-\vec{r}_2|$ then gives

$|\vec{r}-\vec{r}_1| \simeq |\vec{r}| - \hat{n}\cdot\vec{r}_1$. Substitution of the expansion into Eq. (2.14) yields

$$F_n(\vec{\pi}) = \frac{m_1}{2\pi\hbar^2}\iint \frac{\exp(ik_n\pi)\exp(ik_0\hat{\pi}_0\cdot\vec{\pi}_1 - ik_n\hat{\pi}\cdot\vec{\pi}_1)}{\pi-\hat{\pi}\cdot\vec{\pi}_1}$$

$$\times\left(\frac{Z_1Ze^2}{\pi_1} - \frac{Z_1e^2}{\pi_{12}}\right)\psi_n^*(\vec{\pi}_2)\psi_0(\vec{\pi}_2)\,d\vec{\pi}_1\,d\vec{\pi}_2. \qquad (2.15)$$

The fact that $|\vec{r}| \gg |\hat{n}\cdot\vec{r}_1|$ in the denominator implies

$$F_n(\vec{\pi}) = \frac{m_1}{2\pi\hbar^2}\frac{\exp(ik_n\pi)}{\pi}\iint\exp(i(k_0\hat{\pi}_0-k_n\hat{\pi})\cdot\vec{\pi}_1)$$

$$\times\left(\frac{Z_1Ze^2}{\pi_1} - \frac{Z_1e^2}{\pi_{12}}\right)\psi_n(\vec{\pi}_2)\psi_0(\vec{\pi}_2)\,d\vec{\pi}_1\,d\vec{\pi}_2. \qquad (2.16)$$

But by comparison of Eq. (2.1) and Eq. (2.16) we can make the identification

$$F_n(\vec{\pi}) = \frac{m_1}{2\pi\hbar^2}\frac{e^{ik\pi}}{\pi}f(\theta,\phi). \qquad (2.17)$$

Substitution of Eq. (2.16) into Eq. (2.10) yields

$$\sigma_n = \frac{v_1'}{v_1}\frac{m_1^2}{4\pi^2\hbar^4}\left|\iint\exp[i(k_0\hat{n}_0-k_n\hat{n})\cdot\vec{r}_1]\right.$$

$$\left.\times\left(\frac{Z_1Ze^2}{r_1} - \frac{Z_1e^2}{r_{12}}\right)\psi_n^*(\vec{r}_2)\psi_0(\vec{r}_2)\,d\vec{r}_1\,d\vec{r}_2\right|^2. \qquad (2.18)$$

The portion of the scattering amplitude due to the nuclear Coulomb repulsion of the incident projectile is later treated as a perturbation to the scattering cross

section. This approximation is valid since the ionization of the K shell is most likely when the projectile passes at about the K-shell radius r_K. If r_K is large compared to the radius where Coulomb deflection is greatest (where the projectile has reached its radius of closest possible approach), then the probability of strong nuclear Coulomb deflection is small compared to the probability of ionization. The radius of closest approach is, for projectile energy E_1,

$$b = \frac{Z_1 Z e^2}{E_1}, \tag{2.19}$$

while the K-shell radius is

$$r = \frac{\hbar^2}{2m e^2} . \tag{2.20}$$

In terms of the fine structure constant $\alpha = e^2/\hbar c$, we have

$$\frac{b}{r} = \frac{Z_1 Z \alpha^2 m c^2}{E_1} \sim 10^{-2} \tag{2.21}$$

for protons and alphas incident on elements of Z greater than ten for $0.10 < E_1 < 5$ MeV.

The cross section is now given by

$$\sigma_n = \frac{v_1'}{v_1} \frac{m_1^2}{4\pi^2\hbar^4} \left| \iint \exp\left[i(k_0 \hat{r}_0 - k_n \hat{r}) \cdot \vec{r}_1 \right] \right.$$

$$\left. \times \frac{Z_1 e^2}{r_{12}} \psi_n^*(\vec{r}_2) \psi_0(\vec{r}_2) \, d\vec{r}_1 \, d\vec{r}_2 \right|^2 . \tag{2.22}$$

The momentum exchange q is defined as

$$\vec{q} = \vec{k}_0 - \vec{k}_n \; ; \qquad (2.23)$$

so

$$q^2 = k_0^2 + k_n^2 - 2k_0k_n\cos\theta \, , \qquad (2.24)$$

and

$$k_0 k_n = \frac{q\,dq}{\sin\theta\, d\theta} \, . \qquad (2.25)$$

Using Eq. (2.23)-(2.25) and the change of variables $\rho=r_1-r_2$, Eq. (2.22) becomes, after integration over ρ,

$$\sigma_n(q) = \frac{4\pi}{\hbar^2} z_1^2 e^4 \frac{m_1}{E_1} \frac{dq}{q^3} \left| \int \psi_n(\vec{r}_2)\, e^{i\vec{q}\cdot\vec{r}}\, \psi_0(\vec{r}_2)\, d\vec{r}_2 \right|^2 . \qquad (2.26)$$

The total cross section is obtained from Eq. (2.26) by the sum over all initial states of the electron, and the integrals over all possible momentum transfers q and energy transfers E,

$$\sigma = \int_{E_{min}}^{E_{max}} \int_{q_{min}}^{q_{max}} 2\,\sigma_n(q)\, dE\, dq \, . \qquad (2.27)$$

Merzbacher and Lewis[21] have evaluated Eq. (2.27) using hydrogenic wave functions where Z has been replaced by Z_S (the screened nuclear charge as computed by Slater[71]). Since the integral is insensitive to the upper limit, the upper limits of the integration are set equal to infinity.

The lower limit for the momentum exchange is

$$q_{min}^2 = \frac{\varepsilon^2 m_1}{2\hbar^2 E_1} \qquad (2.28)$$

where ε is the observed binding energy of the K-shell electrons.

The minimum energy transfer is equal to the observed binding energy of the K-shell electron. This energy, however, is less than the binding energy given by the hydrogenic Hamiltonian, even when Z is taken to be Slater's screened Z_S. Thus the energy integral must be extended down into the bound hydrogenic states by an amount equal to the difference between the observed and hydrogenic binding energies. Further downward extension of E_{min} to the lowest-lying unoccupied states does not appreciably alter the predicted cross section.[28]

The total K-shell ionization cross section in Eq. (2.27) is given by

$$\sigma_K = \frac{8\pi Z_1^2}{Z_S^4 n_K} f_K a_0^2 , \qquad (2.29)$$

where a_0 is the Bohr radius,

$$n_K = \frac{1}{Z_S^2} \left(\frac{\hbar v_1}{e^2}\right)^2 , \qquad (2.30)$$

and

$$f_K = \int\int \frac{dq}{q^2} \left| \psi_n^*(\vec{r}_2)\, e^{i\vec{q}\cdot\vec{r}_2}\, \psi_K(\vec{r}_2)\, d\vec{r}_2 \right|^2 dE . \qquad (2.31)$$

Merzbacher[21] found that the function f_K can be written as a universal function of η_K / ϕ^2,

$$f_K = f\left(\frac{\eta_K}{\phi^2}\right), \tag{2.32}$$

where

$$\phi = \frac{\mathcal{E}}{Z^2 \, Rydberg} \tag{2.33}$$

and

$$\eta_K = \left(\frac{v_1}{v_{2K}}\right)^2, \tag{2.34}$$

where v_{2K} is the velocity of the K-shell electron. The cross section should then depend only on the projectile's velocity and charge Z_1 and not on its mass. The function given by

$$\left[8\pi a_0^2 \left(\frac{Z_1}{Z_2}\right)^2\right]^{-1} \phi \, \sigma_K \tag{2.35}$$

that is plotted against the variable η_K/ϕ^2 should be the same curve for all targets, projectiles, and energies consistent with the theoretical restrictions. This universal curve has been tabulated by Khandelwal, Choi, and Merzbacher,[72] and will be discussed in Chapter IV. The interpolation routine used on these and following tabulated data was written by R. Lear.[8]

The Binary Encounter Approximation

Due to the well known equivalence of the classical and quantum mechanical Coulomb scattering cross sections, one

might attempt to derive a classical ionization cross section for ion-atom collisions. As in the PWBA, the nucleus provides only the origin of the electron velocity distribution. Thus the name binary encounter approximation (BEA) is derived from the assumption that the only pertinent interaction is the Coulomb force between the incident and target particles (the proton and K-shell electron in this study). As before, the projectile is denoted by the subscript 1, the target electron by the subscript 2. In the laboratory frame, the velocities are given by $\vec{v}_i = v_i \hat{n}_i$ before collision, and $\vec{v}_i' = v_i' \hat{n}_i'$ after collision. In the center-of-mass frame, the velocities are $\vec{v}_{ci} = v_{ci} \hat{n}_{ci}$ and $\vec{v}_{ci}' = v_{ci}' \hat{n}_{ci}'$, as above. If $\vec{V}$ is the velocity of the center of mass, then we have

$$\vec{V} = m^{-1} (m_1 \vec{v}_1 + m_2 \vec{v}_2) \qquad (2.36)$$

and

$$\vec{V} = m^{-1} (m_1 \vec{v}_1' + m_2 \vec{v}_2') , \qquad (2.37)$$

where the total mass is

$$m = m_1 + m_2 , \qquad (2.38)$$

and

$$\vec{V} = \vec{v}_1 - \vec{v}_{c1} . \qquad (2.39)$$

The relative velocities are

$$\vec{v} = v\hat{n} = \vec{v}_1 - \vec{v}_2 \qquad (2.40)$$

and

$$\vec{v}' = v'\hat{n}' = \vec{v}_1' - \vec{v}_2' \quad . \qquad (2.41)$$

The energy exchange ΔE between particles 1 and 2 is

$$\Delta E = \tfrac{1}{2} m_1 v_1'^2 - \tfrac{1}{2} m_1 v_1^2 = \tfrac{1}{2} m_2 v_2^2 - \tfrac{1}{2} m_2 v_2'^2$$

$$= \mu v V (\cos\theta - \cos\theta') , \qquad (2.42)$$

as shown by Gryzinski,[66] where $\mu = m_1 m_2/(m_1+m_2)$ is the reduced mass, and $\bar{\theta}$ and $\bar{\theta}'$ are the polar angles of $\hat{n}$ and $\hat{n}'$, respectively. For given $\vec{v}_1$ and $\vec{v}_2$, the energy exchange depends only on $\underline{\theta}'$ such that

$$d\Delta E = \mu v V \sin\theta' \, d\theta' \, . \qquad (2.43)$$

The total ionization cross section for given $\vec{v}_1$ and $\vec{v}_2$ is $\sigma(\vec{v}_1,\vec{v}_2)$. Gryzinski[66] and Gerjuoy[73] define a differential energy cross section $\sigma_{\Delta E}(\vec{v}_1,\vec{v}_2)$ for the transfer of an amount of energy ΔE by the relation

$$\sigma(\vec{v}_1,\vec{v}_2) = \int_{\Delta E} \sigma_{\Delta E}(\vec{v}_1,\vec{v}_2) \, . \qquad (2.44)$$

But, the cross section is independent of the frame of reference of the observer. So, in terms of the usual center-

of-mass differential cross section $\underline{\sigma}(v;\hat{n},\hat{n}')$, the total cross section is

$$\sigma(\vec{v}_1,\vec{v}_2) = \int d\hat{n}'\,\underline{\sigma}(v;\hat{n},\hat{n}')$$
$$= \int d\underline{\phi}'\,d\underline{\phi}'\,\sin\underline{\theta}'\,\underline{\sigma}(v;\hat{n},\hat{n}')$$
$$= (\mu v V)^{-1}\int d(\Delta E)\,d\underline{\phi}'\,\underline{\sigma}(v;\hat{n},\hat{n}'), \quad (2.45)$$

where $\sin\underline{\theta}'\,d\underline{\theta}' = (\mu v V)^{-1} d(\Delta E)$. Comparing Eqs. (2.44) and (2.45) for $\sigma(\vec{v}_1,\vec{v}_2)$, we have that

$$\sigma_{\Delta E}(\vec{v}_1,\vec{v}_2) = (\mu v V)^{-1}\int d\underline{\phi}'\,\underline{\sigma}(v;\hat{n},\hat{n}'). \quad (2.46)$$

The interaction between the two particles is the Coulomb force; so we may use the well known Rutherford cross section

$$\underline{\sigma}(v;\hat{n},\hat{n}') = \left(\frac{Z_1 Z_2 e^2}{2\mu v^2}\right)^2 \csc^4\left(\frac{\chi}{2}\right), \quad (2.47)$$

where χ is the angle between $\hat{n}$ and $\hat{n}'$. By a straight forward integration, we obtain[73]

$$\sigma_{\Delta E}(\vec{v}_1,\vec{v}_2) = \frac{2\pi (Z_1 Z_2 e^2)^2 V^2}{v^2 |\Delta E|^3}\left(1-\cos^2\underline{\theta}+\frac{\Delta E}{\mu v V}\cos\underline{\theta}\right), \quad (2.48)$$

where

$$-1 < \cos\underline{\theta} - \Delta E/\mu v V \leq 1 \quad (2.49)$$

for energy conservation.

Assume that the velocity distribution of $\vec{v}_2$ is isotropic.

Then, since the cross section in Eq. (2.48) cannot depend on the beam orientation, we may average over the velocities $\vec{v}_1$ and $\vec{v}_2$ to get an effective $\sigma_{\Delta E}(v_1,v_2)$. The expression is

$$\sigma_{\Delta E}^{eff}(v_1,v_2) = \frac{\int d\hat{n}_2\, \sigma_{\Delta E}(\vec{v}_1,\vec{v}_2)}{\int d\hat{n}_1\, d\hat{n}_2\, \frac{(\vec{v}_1 - v_2\hat{n}_2)}{|\vec{v}_1 - v_2\hat{n}_2|}} , \qquad (2.50)$$

where $|\vec{v}_1 - v_2\hat{n}_2| = v$. Reiterating that $\vec{v}_2$ is isotropic, we get

$$\iint d\hat{n}_1\, d\hat{n}_2\, (\vec{v}_1 - v_2\hat{n}_2) = 16\pi^2 v_1 , \qquad (2.51)$$

since $\vec{v}_1$ has a given magnitude. The effective cross section in Eq. (2.50) may now be related to the total cross section by taking an average over the possible values of $\vec{v}_2$, which gives

$$\sigma(v_1,v_2) = \int dv_2\, f(v_2)\, \sigma_{\Delta E}^{eff}(v_1,v_2) , \qquad (2.52)$$

where $f(v_2)$ is an isotropic velocity distribution for the electron shell being ionized. This equation is based on the assumption that particle 1 follows a straight-line trajectory.

The manner in which the function $f(v_2)$ is generated gives rise to the quantal and classical forms of the BEA. Garcia[74] derives a classical distribution from a micro-canonical ensemble. For an electron of binding energy u_K,

the function $f(v_2)$ is

$$f(v_2) = C \int_{\substack{\text{all} \\ \text{space}}} \delta(H-E)\, d^3r$$

$$= C \int_0^\infty \delta\left(\frac{mv_2^2}{2} - \frac{z_2 e^2}{r} + u\right) d^3r. \qquad (2.53)$$

After normalization, we get[74]

$$f(v_2) = \frac{32}{\pi} v_0^5 \frac{v_2^2}{(v_2^2 + v_0^2)^4}, \qquad (2.54)$$

where $v_0 = (2u_K/m)^{\frac{1}{2}}$. The values for the total cross section obtained using Eq. (2.54) may be expressed as a universal curve, as was the case with the PWBA, and have been tabulated by Garcia, Fortner, and Kavanagh.[5]

Hansen[24] used the function $f(v_2)$ derived from hydrogenic momentum space wave functions. The distribution function is then transformed to configuration space to facilitate an impact parameter interpretation. Due to the necessity to restrict the form of the transformed distribution function, this quantum mechanical formulation of the BEA is called the constrained BEA (CBEA).

For medium- and high-Z target atoms, the velocities of the inner shell electrons may be quite relativistic. The velocities would then appear too low, compared to classical predictions. This effect would tend to raise the ionization cross section. The CBEA is corrected approximately for relativistic effects by replacing the value of v_2 found

above through a non-relativistic distribution function with

$$v_2' = [R/(1+R)]^{\frac{1}{2}} c \qquad (2.55)$$

the velocity inferred from the total relativistic energy of the electron, where

$$m = m_0/(1-\beta^2)^{\frac{1}{2}}, \qquad (2.56)$$

with

$$R = (E_2/m_0c^2)^2 + 2(E_2/m_0c^2), \qquad (2.57)$$

and

$$\beta = \frac{v_2'}{c} \quad . \qquad (2.58)$$

Hansen's calculations[44] show that for the highest Z_2 (=46) and lowest energy E_1 (=0.4 MeV) used in this work[10], the relativistic correction will raise the estimated cross section by 30 per cent.

The CBEA is limited to proton energies greater than 1.0 MeV, due to the method used to transform the BEA to configuration space. Hansen[24] assumes that the momentum-space and configuration-space wave functions may be related by

$$\int_{v'}^{0} \phi^*(v)\,\phi(v)\,v^2\,dv = \int_{n'}^{\infty} \psi^*(n)\,\psi(n)\,n^2\,dn, \qquad (2.59)$$

where $\phi(v)$ is the velocity-space wave function, $\psi(r)$ is the configuration-space wave function, and v' is the velocity a classical particle would have at r'. The correct relationship is given by

$$\int_{n'}^{\infty} \psi^*(n)\,\psi(n)\,n^2\,dn = \int_0^{\infty}\int_0^{\infty}\int_{n'}^{\infty} \phi^*(v_1)\,\phi(v_2)\,(i\,n\Delta p)^{-1}$$

$$\times\left(e^{i n\Delta p} - e^{-i n\Delta p}\right) v_1^2\,dv_1\,v_2^2\,dv_2\,n^2\,dn, \quad (2.60)$$

where $\Delta p = |\vec{p}_2 - \vec{p}_1|$. It is not evident how the triple integral can be replaced by the single integral over the velocity. The effects of using Eq. (2.59) are discussed in Chapter IV.

Corrections to the PWBA

In the opening paragraphs on the PWBA, we assumed that the incident proton was not deflected by the Coulomb field of the target nucleus, and that the electron states were undisturbed by the proton's presence. Yet, these effects do exist and are significant in the low-energy region below 1.0 MeV. Basbas, Brandt, and Laubert[22] have given an approximate treatment of these effects for protons incident on moderate Z targets.

In fact, the incident proton is deflected by the Coulomb field of the nucleus so that its distance of closest approach to the nucleus is greater than that expected if deflection is ignored. The resulting ionization cross section would be

decreased, since the proton would sample less of the electron distribution. Simultaneously, the proton velocity decreases as it approaches the repulsive potential. The relative velocity of the proton and electron would increase and the resulting cross section would be further depressed.

The slower the proton is moving, the longer it is within the K-shell radius. When this transit period approaches the response time of the K-shell electrons, the electron binding energy increases while the proton is present. This increased binding means that the electron virial velocity increases, consequently the relative velocity increases; so that the cross section in Eq. (2.29) is once more decreased. The three effects have been summarized by Basbas et al.[22] in the equation

$$\sigma_K = \sigma_K^{PWBA}(\eta_K; \varepsilon\phi_K)\, 9E_{10}(\pi\varepsilon d_{q_0}), \qquad (2.61)$$

where σ_K is the corrected cross section of Eq. (2.29), η_K and ϕ_K are defined by Eqs. (2.34) and (2.33), respectively, and $\varepsilon = 1 + \Delta E_1/E_1$ is the fractional change in the energy of the proton due to the repulsive Coulomb potential of the target nucleus. The function $E_{10}(x)$ is the tenth order exponential integral defined by

$$E_{10}(x) = \int_1^\infty t^{-10} e^{-xt}\, dt . \qquad (2.62)$$

The Relativistic PWBA

The inner shell electrons of medium-and high Z-atoms have significant probabilities of having velocities close to the speed of light. It would appear that one would need to use the Dirac equation to treat these electrons relativistically, which would give the relativistic PWBA (PWBAR). In place of the hydrogenic wave functions used in the PWBA, one should use the Dirac hydrogenic wave functions.[75,76] Jamnik and Zupancic[25] have investigated this approach for K-shell ionization of lead and silver by protons. They begin with the expression for the differential energy cross section,

$$\sigma = \frac{4\pi}{\hbar^2} Z_1^2 e^4 \frac{m_1}{E_1} \int_{q_{min}}^{\infty} J \frac{dq}{q^3} , \qquad (2.63)$$

where q_{min} is the minimum momentum exchange and is given by

$$q_{min} = \frac{\epsilon^2 m_1}{2\hbar^2 E_1} , \qquad (2.64)$$

and ϵ is the observed binding energy. The function J is

$$J = \sum_f \left[\int e^{i\vec{q}\cdot\vec{r}} \psi_i(\vec{r}_2) \psi_f^*(\vec{r}_2) d\vec{r}_2 \right]^2 , \qquad (2.65)$$

where the sum is over the final electron states, the integral is over the electron coordinates r_2, $\psi_i(\vec{r}_2)$ is the initial electron wave function, and $\psi_f(\vec{r}_2)$ is the final electron wave function.

The functions $\psi_i(\vec{r}_2)$ and $\psi_f(\vec{r}_2)$ are solutions of the Dirac equation[77]

$$i\hbar \frac{\partial}{\partial t} \psi(\vec{r}_2) = \left(c\vec{\alpha}\cdot\vec{p} + \beta mc^2 - \frac{Ze^2}{r_2}\right)\psi(\vec{r}_2), \quad (2.66)$$

where c is the speed of light. The 4x4 matrices

$$\vec{\alpha} = \begin{bmatrix} 0 & \vec{\sigma} \\ \vec{\sigma} & 0 \end{bmatrix}, \quad (2.67)$$

and

$$\beta = \begin{bmatrix} 1 & 0 \\ 0 & -1 \end{bmatrix}, \quad (2.68)$$

are given in terms of the Pauli spin matrices σ

$$\sigma_x = \begin{bmatrix} 0 & 1 \\ 1 & 0 \end{bmatrix}; \quad \sigma_y = \begin{bmatrix} 0 & -i \\ i & 0 \end{bmatrix}; \quad \sigma_z = \begin{bmatrix} 1 & 0 \\ 0 & -1 \end{bmatrix}.$$

Explicit form of the functions for the bound and continuum states is given by Rose.[75,76] Substitution of these functions into the expression for J gives

$$J = \sum_f |n_f| \left[A q^{-(\gamma_i+\gamma_f+1)} S(\varepsilon_i/q)\right]^2, \quad (2.69)$$

where A is a final state dependent constant, $\gamma_i = (|\eta|^2 - (\xi Z)^2)^{1/2}$, ξ is the fine structure constant, η is the relativistic principal quantum number, and $S(\varepsilon/q)$ is a polynomial in ε/q (ε is the binding energy expressed in units of inverse length.). Jamnik and Zupančič[25] performed the indicated integrals and sums for lead and silver. For silver at E_1= 1.7 MeV, the

cross section was found to be 30 per cent higher than the value predicted by the non-relativistic PWBA.

Bang and Hansteen[65] have made an approximate expansion of the above polynomial,keeping terms only through ε/q. They found that the PWBAR gives consistently higher values for the cross section. The ratio of PWBAR to PWBA cross sections is found to increase with decreasing E_1, since for lower values of v_1, the proton must sample the higher-velocity (more relativistic) electrons in order to transfer enough energy to ionize the electron.

CHAPTER III

EXPERIMENTAL PROCEDURE

The physical situation under study is the production of characteristic x rays due to proton bombardment of medium-Z elements. The experimental apparatus, discussed previously[8, 10,12,15] has been used in all the x-ray production studies made at the Regional Nuclear Physics Laboratory at North Texas State University. The proton flux is generated by the Laboratory's 2-MV Van de Graaff accelerator. The energy of the proton beam is determined by the strength of the magnetic field needed to bend the direction of the beam by 25 degrees. The calibration of proton energy versus magnetic field strength for this bending angle was made by determining the threshold of the $^{7}Li(p,n)^{7}Be$ reaction as reported by Roush *et al.*,[78] and the positions of the $^{27}Al(p,\gamma)^{28}Si$ resonance reactions measured by Lyons *et al.*,[79] and Roush *et al.*[78] The magnetic field is measured using a Hall probe that is permanently attached to the beam line and is located near the center of the pole pieces. The proton energy is given by

$$E = c\,(\text{Hall Probe Voltage})^{2}, \qquad (3.1)$$

where c is determined from the threshold measurements. The calibration error is ±5 keV and arises from the statistical

significance of the threshold data, thermal fluctuations of the Hall probe coefficients, and beam divergence due to the finite width of the collimation slits.

Leaving the magnet, the proton beam then passes through a liquid-nitrogen cold trap (see Fig. 1.) designed to reduce the transfer of carbon contaminants from the Van de Graaff vacuum system into the target chamber. Later analysis[8] has shown that contaminant accumulation, even over long periods of exposure, is negligible. The beam then passes between the energy regulation slits, which also provides horizontal definition of the beam. The second set of slits provide vertical definition. The beam then passes through the transmission-mounted target and is collected in a Faraday cup. The beam intensity is measured using standard current integration techniques.

The target is placed at 45 degrees with respect to the beam. When the target is placed at this angle, the incident proton passes through the same amount of target material as the outgoing x ray. If the targets are sufficiently thick to significantly attenuate the flux, the use of this geometry simplifies correction equations.[5,22] But the use of thin targets circumvents the need of these corrections. For example, the thickest target studied was 44.1 $\mu g/cm^2$ of Pd. The mass absorption coefficient[80] of Pd for its own x rays is 9 cm^2/g. Now, for thin samples, the intensity of radiation passing through matter falls off exponentially. We may express this attenuation by the following[81]:

$$I = I_0 e^{-\mu x}, \qquad (3.2)$$

where I is the intensity after the incident flux I_0 has traversed an amount of material x (g/cm^2). Thus the attenuation of the Pd x-ray flux is about 0.01 percent, which is negligible.

Protons backscattered from the target are observed by a 1000-μ Si surface-barrier detector (see Fig. 2.) placed at 168 degrees with respect to the beam. The detector is partially shielded by a 1.5-mm Mo collimator. The collimator is centered over the active region of the detector. The detector's solid angle, as seen from the intersection of the beam and the target (the beam spot) was measured by two methods as a check. First, the geometrical solid angle was calculated, using the measured diameter of the collimator d and the distance to the beam spot s. The solid angle Ω is given by

$$\Omega = \frac{\pi\left(\frac{d}{2}\right)^2}{4\pi s^2}. \qquad (3.3)$$

Secondly, a ^{244}Cm α emitter with an intensity known to within 2 per cent and with a source distribution similar to the beam spot was placed in the target position. The scattering chamber was evacuated and the apparent activity of the source was measured with the collimated detector. The solid angles determined by the two methods agreed to

within experimental error of ±3 per cent.

The Si(Li) x-ray detector is mounted externally to the vacuum system at 90 degrees with respect to the beam. The detector has a resolution of 168 eV at 5.898 keV and a 0.0127-mm beryllium window. There is a 0.0127-mm Mylar vacuum window and a 0.25-mm Mylar absorber between the detector and the target. The absorber is necessary to reduce the copious L x-ray flux from the target. A typical x-ray spectrum is found in Fig. 3. Note that the $K\alpha_1$ and $K\alpha_2$ peaks are unresolved. The $K\beta_1$, $K\beta_3$, and $K\beta_5$ peaks are unresolved and are labeled $K\beta_1$. The $K\beta_{2,4}$ peak is resolved from the $K\beta_1$ peak. The Kα peak-to-background ratio is 200/1,rendering peak integration analysis insensitive to the methods used in background subtraction.

The efficiency of the Si(Li) detector system was found as a function of photon energy by using standardized sources of ^{51}Cr, ^{54}Mn, ^{57}Co, ^{65}Zn, and ^{241}Am obtained from the Oak Ridge Associated Universities. The intensity of a particular gamma ray for a given source is calibrated to within 3 per cent. The relative intensities of the remaining gamma and x rays must then be taken from the literature.[82,83] The sources are then mounted in the target position, and counted under experimental conditions. The ratio of the measured x-ray flux to the known flux from the source is the detector system efficiency. This method takes into account absorption in both Mylar sheets, the Be detector window, the air path, the insensitivity of the surface of

the detector, and geometrical factors. The source distribution is similar in size to the beam spot, both being small enough to make source distribution geometrical corrections negligible. The sources are 4-mm^2 lamina sealed between 0.127-and 0.0127-mm thick sheets of Mylar. Absorption by the Mylar of the characteristic x rays is less than 0.1 per cent. The source distribution closely approximates the actual beam spot. Later experiments where the beam dimensions were varied by factors of two revealed no discernible effect under identical experimental conditions on the measured x-ray production cross sections. The accuracy of the efficiency measurements may be estimated from the known uncertainties. The original intensity calibration had an error of ±3 per cent, the relative intensities ±2 per cent, and the statistical fluctuation for each x ray ±1 per cent. The expected error is 3.7 per cent. The detector system efficiency is shown in Fig. 4.,where the solid curve is an eye guide. For purposes of error assignment later in this paper, we assign an overall error to the efficiency of ±5 per cent.

The transmission-mounted targets consist of self-supporting carbon foils onto which target materials have been vacuum evaporated,using standard techniques.[84] The target and carbon foil thicknesses were measured by counting the number of Rutherford backscattered protons for given proton bombarding energy and total incident charge. The target thickness is then given by the following

$$\rho = \frac{16 E^2 \sin^4(\frac{\theta}{2})}{Z^2 e^4} N_C \frac{A}{C}, \qquad (3.4)$$

where ρ is the mass per unit area upon which a total charge C was incident. The incident protons have energy E, charge e, and are scattered through the angle θ (168 degrees). The target has atomic weight A and charge Ze. The scattered yield is N_C. The target thicknesses are listed in Table I. Energy loss by the beam in the thickest target, Pd, is 0.1 per cent at 2.0 MeV. Thus corrections for beam energy degradation are not necessary.

The electronics used for data acquisition are shown in Fig. 5. The output of each detector is routed to a multichannel analyzer (MCA). The analyzers are gated by the current integrator so that the analyzers will accept input pulses only when the integrator is counting the charge incident on the target. But the contrary is not true. During the time the MCA is analyzing a pulse, additional incoming pulses are not counted. This dead time of the MCA must be corrected for when computing the actual number of pulses received from the respective detector. In order to make the correction small, the total flux of protons must be low. For the present experimental arrangement, the beam intensity was kept below 200 na at 2.0 MeV and below 100 na at 1.0 MeV. Thus the deadtime for both detectors was kept below 5 per cent.

The above experimental procedure possesses an advantage

beyond the convenience of the gated analyzers. Note that when one takes the ratio of the x-ray yield Y_x to the Rutherford yield Y_R in Eq. (3.5), the beam flux and the target density cancel, since they are the same for each detector. We are left with the relation

$$\frac{Y_x}{Y_R} = \frac{\sigma_x \varepsilon}{\sigma_R \Omega} , \qquad (3.5)$$

where σ_x is the x-ray cross section, ε is the x-ray detector efficiency, Ω is the particle detector solid angle, and σ_R is the Rutherford cross section. The values of σ_x is then given by

$$\sigma_x = \frac{\Omega}{\varepsilon} \frac{Y_x}{Y_R} \sigma_R . \qquad (3.6)$$

Problems involving target uniformity, target evaporation, beam optics, and beam fluctuations do not influence the measured cross section.

The ionization cross section σ_I is related to σ_x by the fluorescence yield ω_K. The theoretical values of ω_K, calculated by Kostroun,[85] are given in Table II. They agree with the experimental values given in the review article by Bambynek, et al.,[60] but Kostroun's values are used in this work.

Larkins[62] has shown that ω_K changes only 10 per cent for the vacancy configuration (1s,2p) in argon. Richard, et al.,[61] have reported that for 800 keV protons on Ti there is less than 10 per cent multiple ionization. Thus the average value of ω_K should be very close to the single ionization coefficient ω_{K0}.

CHAPTER IV

DISCUSSION OF RESULTS

The measured values of the x-ray production cross sections are presented in Table III. The ionization cross sections given in the adjacent column of this table were obtained using the values of ω_K reported by Kostroun.[85] The errors quoted in the ionization cross sections include the statistical errors of the observed Kα and Kβ x-ray intensities (1-4 per cent) and backscattered proton intensity (1 per cent), uncertainties in the strengths of the calibration sources (3 per cent), statistical fluctuations in the yields of the calibration measurements (1-2 per cent), and the experimental uncertainties in the flourescence yields[60] (5 per cent). The total error in the measured ionization cross sections is typically 8 per cent.

The Kα/Kβ ratios, corrected for efficiency, were observed to be constant for a given element over the proton energy range of this study. The average values of Kα/Kβ are given in Table IV. These measured ratios agree to within experimental uncertainties with the calculated values of Scofield.[86] The measured values also agree to within the error limits with the experimental values given for Rb by Close, et al.,[87] Hansen,[88] and Rao, et al.[89]

The data are plotted in Fig. 6. in a universal curve representation from Eqs. (2.32)-(2.35), $u_K\sigma_I$ versus $E_1/\lambda u_K$, where u_K is the K-shell ionization energy, σ_I is the ionization cross section, and λ is the ratio of the proton mass to the electron mass. The data lie within ±8 per cent of a curve that increases smoothly with increasing projectile energy. The data are compared to previous measurements in Table III. The values generally agree to within experimental error. The widest variation is with the 1.0-MeV value for Rb given by Bearse.[26] Given the overall good self-consistency of the data in the present work and the good agreement with the bulk of the previous data, I believe this particular measurement reported by Bearse to be too low.

The theoretical values for the ionization cross sections are plotted in Fig. 6. The non-relativistic PWBA given by Khandelwal, Choi, and Merzbacher[28] in Eq. (2.32) is labeled PWBA. The remaining theoretical curves are also labeled as in the text. The PWBA is seen to lie 20 per cent above the data at $E_1/\lambda u_K$=0.070, but is 60 per cent above the data at 0.015. The CBEA is a few per cent high over most of the energy range, but falls well below the data below the point at $E_1/\lambda u_K$=0.020. This result suggests that above 1.0 MeV the proton velocity sufficiently approximates the upper limit of infinity in Eq. (2.59), and the distance r', which must be on the order of the K-shell radius such that the probability for ionization is significant, is close enough to zero so that the quotient containing the exponential

terms in Eq. (2.60) approximates a delta function. The BEA falls 10 percent below the data in the range greater than 0.030. Below 0.030 the data decreases faster than the BEA. The PWBAC is 5 per cent below the data at 0.080 and gradually falls to 15 per cent below the data at 0.010. The shape of the PWBAC most nearly coincides with the energy dependence of the data. These trends may be more easily observed in Fig. 7 , where $\sigma_{I\ Experimental}/\sigma_{I\ Theoretical}$ is plotted as a function of $E_1/\lambda u_K$ for the elements Se and Pd. The curves shown in Fig. 7 are guides for the eye. The divergence between the data and the PWBAC as E_1 decreases suggests the need for relativistic corrections to the PWBA. The relativistic corrections increase as E_1 decreases because the proton must encounter increasingly higher velocity electrons so that an amount of energy greater than u_K may be transferred to the electron. These high-velocity electrons require the more accurate relativistic description.

The measured $K\alpha/K\beta$ ratios agree with Scofield's calculations; so we conclude that the earlier assumption of small multiple ionization probabilities is correct. If large numbers of vacancies were produced, the radiative widths would have changed noticeably.[62] Thus, differences between the data and the various theories do not depend on ω_K, but must arise from assumptions made in the basic theories. I anticipate that a combination of the Brandt corrections[22] and the relativistic PWBA will most accurately describe the K-shell ionization by proton bombardment.

APPENDIX: THE RELATIVISTIC PLANE-WAVE BORN APPROXIMATION

The following development of the relativistic plane-wave Born approximation is based on the paper by Jamnik and Zupančič.[25] We assume that the first Born approximation as developed in Eq. (2.26) is applicable to the ionization of K-shell electrons by protons. Expressed in terms of the energy of the ejected electron E_f, the differential cross section is

$$\frac{d\sigma(q)}{dE_f} = \frac{4\pi}{\hbar^2} Z_1^2 e^4 \frac{m_1}{E_1} \frac{dq}{q^3} \left| \int \psi_n(\vec{r}_2) e^{i\vec{q}\cdot\vec{r}} \psi_0(\vec{r}_2) d\vec{r}_2 \right|^2 . \quad (2.26)$$

However, in place of the non-relativistic electron wave functions used in Eq. (2.26), we use the relativistic electron wave functions obtained from Eq. (2.66). The differential energy transfer cross section is rewritten as

$$\frac{d\sigma}{dE_f} = \frac{4\pi}{\hbar^2} Z_1^2 e^4 \frac{M_1}{E_1} \int_{q_{min}}^{q_{max}} J \frac{dq}{q^3} \quad (A.1)$$

where Z_1, E_1, and M_1 are the charge, energy, and mass of the proton. $\hbar q$ is the momentum exchange. The minimum momentum exchange q_{min} that can produce ionization is related to the observed binding energy ε by the conservation of energy

$$\hbar^2 q_{min}^2 \simeq 2M_1 (\sqrt{E_1} - \sqrt{E_1 - \varepsilon})^2 \simeq \frac{1}{2} M_1 \frac{\varepsilon^2}{E_1} .$$

Likewise, the maximum momentum transfer is

$$\hbar^2 q_{max}^2 = 2M_1\left(\sqrt{E_1} + \sqrt{E_1 - \varepsilon}\right)^2 \simeq 8M_1E_1 ,$$

but for all practical purposes we may set $q_{max} = \infty$. The quantity J is given by

$$I = \sum_{\eta_f}\left[\int e^{i\vec{q}\cdot\vec{r}}\,\psi_f^*(\vec{r})\,\psi_i(\vec{r})\,d\vec{r}\right]^2 \qquad (A.2)$$

where $\psi_i(\vec{r})$ and $\psi_f(\vec{r})$ are the initial and final wave functions of the electron, respectively. The electron wave functions can be written

$$\psi(\vec{r}) = \begin{pmatrix} -i f_\eta(r)\,\chi_{-\eta}^{\mu}(\theta,\phi) \\ g_\eta(r)\,\chi_{\eta}^{\mu}(\theta,\phi) \end{pmatrix} \qquad (A.3)$$

where $\eta = \pm 1, \pm 2, \cdots$. The two componant spinors may be written in terms of the orbital angular momentum by[90]

$$\chi_\eta^\mu = \sum_\tau \left\langle l(\eta), \tfrac{1}{2}, \mu-\tau, \tau \middle| l(\eta), \tfrac{1}{2}, j, \mu\right\rangle \times \chi_{\frac{1}{2}}^{\tau}\, Y_{l(\eta)}^{\mu-\tau}(\theta,\phi) , \qquad (A.4)$$

where

$$j = |\eta| - \tfrac{1}{2} \qquad l(\eta) = \eta \quad \text{if } \eta > 0$$

$$-j \le \mu \le j \qquad l(\eta) = |\eta| - 1 \quad \text{if } \eta < 0$$

and

$$\chi_{\frac{1}{2}}^{\frac{1}{2}} = \begin{pmatrix} 1 \\ 0 \end{pmatrix} \qquad \chi_{\frac{1}{2}}^{-\frac{1}{2}} = \begin{pmatrix} 0 \\ 1 \end{pmatrix} .$$

The functions $Y_{\ell}^{m}(\theta,\phi)$ are the spherical harmonics. The Clebsch-Gordon coefficient is the expansion coefficient of χ_{η}^{μ} for the angular momentum eigenfunction Y_{ℓ}^{m}.

The radial wave functions are written in the usual manner

$$f_n(r) = D\, r^{-1}\, u(r)$$
$$g_\eta(r) = D\, r^{-1}\, v(r) . \qquad (A.5)$$

Bethe[91] has solved Eq. (2.66) for these quantities for the discrete states and obtained

$$u(r) = -\sqrt{1-\Theta}\; r^{\gamma_n} e^{-\varepsilon_N r}\left[n' \Phi(-n'+1, 2\gamma_\eta+1, 2\varepsilon_N r) + (N-\eta)\,\Phi(-n', 2\gamma_\eta+1, 2\varepsilon_N r)\right]$$

and

$$v(r) = \sqrt{1+\Theta}\; r^{\gamma_\eta} e^{-\varepsilon_N r}\left[-n' \Phi(-n'+1, 2\gamma_\eta+1, 2\varepsilon_N r) + (N-\eta)\,\Phi(-n', 2\gamma_\eta+1, 2\varepsilon_N r)\right] . \qquad (A.6)$$

In Eq. (A.6) the quantities

$$\Theta = \frac{E}{mc^2} = \left[1 + \frac{(\xi Z)^2}{(\eta'+\gamma_\eta)^2}\right]^{-\frac{1}{2}}$$

$$\gamma_\eta = \sqrt{|\eta|^2 - (\xi Z)^2}$$

$$\varepsilon_N = Z(Na_0)^{-1}$$

$$N = \sqrt{n^2 - 2n'(|\eta| - \gamma_\eta)}$$

$$n = n' + |\eta|$$

$$D = \sqrt{\frac{\Gamma(2\gamma_\eta + n' + 1)}{4(n'!)N(N-\eta)}} \quad \frac{(2\varepsilon_N)^{\gamma_\eta + \frac{1}{2}}}{\Gamma(2\gamma_\eta + 1)}$$

are used, where a_0 is the Bohr radius, $\xi = e^2/hc$ is the fine structure constant, and E the total energy of the electron. Φ is the confluent hypergeometric function, regular at the origin. For the initial state of the K-shell electron, we have $\eta = -1$, and $n' = 0$, and

$$f_i(r) = -\sqrt{1-\gamma_i}\, C\, r^{\gamma_i - 1} e^{-\varepsilon_i r} \qquad (A.7)$$

$$g_i(r) = \sqrt{1+\gamma_i}\, C\, r^{\gamma_i - 1} e^{-\varepsilon_i r}$$

where the normalization constant C is obtained from

$$\int \psi^* \psi \, d\vec{r} = \int_0^\infty (f_i^2 + g_i^2) r^2 dr = 1,$$

and is given by

$$C = \frac{(2\varepsilon_i)^{\gamma_i + \frac{1}{2}}}{\sqrt{2\Gamma(2\gamma_i + 1)}}.$$

Rose[76] has solved Eq. (2.66) for the continuum wave functions and obtained

$$u(r) = -2\sqrt{W-1}\, r^{\gamma_\eta}\, \mathrm{Im}\left[e^{-ikr+i\eta(\gamma_\eta+i\alpha)} \times \Phi(\gamma_\eta+1+i\alpha, 2\gamma_\eta+1, 2ikr)\right]$$

$$v(r) = 2\sqrt{W+1}\, r^{\gamma_\eta}\, \mathrm{Re}\left[e^{-ikr+i\eta(\gamma_\eta+i\alpha)} \times \Phi(\gamma_\eta+1+i\alpha, 2\gamma_\eta+1, 2ikr)\right] \qquad (A.8)$$

where

$$e^{2i\eta} = -\frac{\eta - i\beta}{\gamma_\eta + i\alpha}$$

$$\beta = \varepsilon_1 / k$$

$$\alpha = \beta W$$

$$W = \frac{E}{mc^2} = \left(1 + \left(\frac{k\hbar}{mc}\right)^2\right)^{\frac{1}{2}}$$

and

$$D = \frac{2^{\gamma_\eta - 1}}{\Gamma(2\gamma_\eta+1)\hbar} \sqrt{\frac{m}{LW}}\, k^{\gamma_\eta}\, e^{\frac{\pi\alpha}{2}} \left|\Gamma(\gamma_\eta + i\alpha)\right| .$$

In Eq. (A.8) Im denotes the imaginary, and Re the real, part of the expression in parentheses. The continuum wave function is box-normalized in a volume of dimension L. The box-normalized wave functions of Eq. (A.8) are compatible with the bound state wave functions of Eq. (A.7), since L may be chosen sufficiently large that the contribution of the bound state wave functions beyond r=L is

negligible. The integral over $\vec{r}$ in Eq. (A.2) may be understood to be over the volume of the "large" box. The volume of the box may then become infinite after the r integration, since the volume divides out.

By substitution, Eq. (A.2) becomes

$$\mathcal{I} = \sum_{\zeta} \left[\int e^{i\vec{q}\cdot\vec{r}} \left(f_{\zeta}^{*} f_i \chi_{-\zeta}^{\mu *} \chi_{-i}^{\mu} + g_{\zeta}^{*} g_i \chi_{\zeta}^{\mu *} \chi_{i}^{\mu} \right) d\vec{r} \right]^2 . \quad (A.9)$$

The sum over the final magnetic quantum numbers and average over the initial magnetic quantum numbers are performed by Rose and Osborn[75] and lead to their Eq. (54). Integration over the angles then yields (see Eq. (11.7.8) of Ref. 70)

$$\mathcal{I} = \sum_{\zeta} |\eta_{\zeta}|^2 \left\{ \int_0^{\infty} j_{l(\zeta)}(qr) \left[f_i f_{\zeta}^{*} + g_i g_{\zeta}^{*} \right] r^2 dr \right\}^2 , \quad (A.10)$$

where $j_l(qr)$ is the spherical Bessel function.

The radial integration may be done by expressing the function $j_l(qr)$ as a confluent hypergeometric Φ (see Eq. (6.9.9) of Ref. 92):

$$j_l(x) = \frac{\sqrt{\pi}\, x^l e^{-ix}}{\Gamma(l+\frac{3}{2})\, 2^{l+1}} \Phi(l+1, 2l+2, 2x) . \quad (A.11)$$

Using the integral representations for Φ (see Eq. (6.5.1) of Ref. 92), the K-shell functions for g_i and f_i, and Eq. (A.8) for the continuum states f_f and g_f, Jamnik and Zupancic[25] performed the radial integration to obtain

$$I = \int_0^\infty j_l(qr)\left[f_{\xi}^{*} f_i + g_{\xi}^{*} g_i\right] r^2 dr$$

$$= \frac{\sqrt{\pi}\,\Gamma(2a)}{\Gamma(l+\tfrac{3}{2})}\, CD \left(\frac{q}{2}\right)^{l} \mathrm{Re}\left\{ X (\varepsilon_1 + ik + iq)^{-2a} \right.$$

$$\times F_2\left(2a, l+1, \gamma_{\xi}+1+i\alpha, 2l+2, 2\gamma_{\xi}+1;\right.$$

$$\left.\left. \frac{2iq}{\varepsilon_1 + ik + iq}, \frac{2ik}{\varepsilon_1 + ik + iq} \right)\right\} \qquad (A.12)$$

where F_2 is defined by Eq. (5.8.1) of Ref. 92 as

$$F_2(\alpha, \beta, \beta', \gamma, \gamma'; x, y) = \frac{\Gamma(\gamma)\,\Gamma(\gamma')}{\Gamma(\beta)\,\Gamma(\beta')\,\Gamma(\gamma-\beta)\,\Gamma(\gamma'-\beta')}$$

$$\times \int_0^1 \int_0^1 u^{\beta-1} v^{\beta'-1} (1-u)^{\gamma-\beta-1} (1-v)^{\gamma'-\beta'-1} (1-ux-vy)^{-\alpha} dv\, du$$

$$\mathrm{Re}\,\beta > 0, \quad \mathrm{Re}\,\beta' > 0, \quad \mathrm{Re}(\gamma-\beta) > 0, \quad \mathrm{Re}(\gamma'-\beta') > 0$$

for

$$a = \frac{\gamma_1 + \gamma_{\xi} + l + 1}{2}$$

and

$$X = \left(\sqrt{w+1}\sqrt{1+\gamma_1} - i\sqrt{w-1}\sqrt{1-\gamma_1}\right)(\gamma_{\xi}+i\alpha)\, e^{i\eta}.$$

F_2, in turn, may be used to define the function H_4 by the relation[93]

$$F_2(\alpha,\beta,\beta',2\beta,\gamma';x,y)$$

$$=(1-\tfrac{x}{2})^{-\alpha}\,H_4(\alpha,\beta',\beta+\tfrac{1}{2},\gamma';\frac{x^2}{4(2-x)^2};\frac{2y}{2-x}). \quad (A.13)$$

Eq. (A.12) becomes

$$I=\frac{\sqrt{\pi}\,\Gamma(2a)}{\Gamma(l+\frac{3}{2})}\,C\,D\,(\tfrac{q}{2})^{l}\,\mathrm{Re}\{X\,(\varepsilon_1+ik)^{-2a}$$

$$\times H_4(2a,\gamma_f+l+i\alpha,l+\tfrac{3}{2},2\gamma_f+H;-\frac{q^2}{4(\varepsilon_1+ik)^2},\frac{Z_i k}{\varepsilon_1+ik})\}. \quad (A.14)$$

From Eq. (5.7.16) of Ref. 92, H_4 may be written

$$H_4(\alpha,\beta,\gamma,\delta;x,y)=\sum_{m,n}\frac{(\alpha)_{2m+n}\,(\beta)_m}{(\gamma)_m\,(\delta)_n\,m!n!}\,x^m y^n$$

$$=\sum_m\frac{(\alpha/2)_m\,(\frac{\alpha+1}{2})_m}{(\gamma)_m\,m!}\,F(\alpha+2m,\beta,\gamma,y)\,(4x)^m$$

where $(a)_n$ is the Pochhammer symbol

$$(a)_n=a(a+1)\cdots(a+n-1)$$

and F(a,b,c,y) is the hypergeometric function given by Eq. (2.1.4) of Ref. 92.

For low proton bombarding energies ($\sim$1 MeV) and medium Z elements, there must be large momentum transfers (i.e., $q/\varepsilon_1 \simeq 1$) to ionize the K-shell electrons. We must require analytic continuation in the variable x which is

proportional to q/ε_1, since Eq. (A.15) diverges for x greater than one. Using the usual continuation relation (e.g., Eq. (2.1.17) of Ref. 92) in Eq. (A.15), we obtain

$$H_4(\alpha,\beta,\gamma,\delta;x,y) = \frac{\Gamma(\frac{1}{2})\,\Gamma(\gamma)}{\Gamma(\frac{\alpha+1}{2})\,\Gamma(\gamma-\frac{\alpha}{2})}\,(-4x)^{-\frac{\alpha}{2}}$$

$$\times\left[\sum_m \frac{(\frac{\alpha}{2})_m\,(1-\gamma+\frac{\alpha}{2})_m}{(\frac{1}{2})_m\,m!}\,F(-2,\beta,\delta,y)(4x)^{-m}\right]$$

$$+\frac{\Gamma(-\frac{1}{2})\,\Gamma(\gamma)}{\Gamma(\frac{\alpha}{2})\,\Gamma(\gamma-\frac{\alpha+1}{2})}(-4x)^{-\frac{\alpha+1}{2}}\left[\sum_m \frac{(\frac{\alpha+1}{2})_m\,(\frac{3}{2}-\gamma+\frac{\alpha}{2})_m}{(\frac{3}{2})_m\,m!}\right.$$

$$\left.\times F(-2m-1,\beta,\delta,y)(4x)^{-m}\right]. \qquad (A.16)$$

Substitution of Eq. (A.16) into Eq. (A.14) yields

$$I = A\,q^{-(\gamma_1+\gamma_2+1)}\;S(\varepsilon,k),$$

where

$$S(x) = F\sum_m P_m(-1)^m x^{2m} + G\sum_m Q_m(-1)^m x^{2m+1}$$

$$F = \frac{\Gamma(c)}{\Gamma(a+\frac{1}{2})\,\Gamma(1-b)}$$

$$G = \frac{\Gamma(c-1)}{\Gamma(a)\,\Gamma(\frac{1}{2}-b)}$$

$$A = B D_f$$

$$B = C \frac{\sqrt{\pi}\,\Gamma(a)}{2^{l+1}}$$

$$P_m = \frac{(a)_m (b)_m}{(c)_m m!} p_m$$

$$Q_m = \frac{(a+\frac{1}{2})_m (b+\frac{1}{2})_m}{(c+1)_m m!} q_m$$

$$b = \frac{\gamma_i + \gamma_f - l}{2}$$

$$d = \frac{1}{2}$$

The quantities p_m and q_m are descriptive of the final state. For the final state being in the continuum, we have

$$p_m = 2\,\mathrm{Re}\{ F(-2m, \gamma_f + 1 + i\alpha, 2\gamma_f + 1, y)\, v^{2m} \chi \}$$

$$q_m = 2\,\mathrm{Re}\{ F(-2m-1, \gamma_f + 1 + i\alpha, 2\gamma_f + 1, y)\, v^{2m+1} \chi \}$$

$$y = \frac{2ik}{\varepsilon_1 + ik}$$

$$v = 1 + i\frac{k}{\varepsilon_1} \,,$$

which are Eqs. (11) and (13) in Ref. 25. A similar development holds for the discrete case where f_f and g_f are discrete states given by Eq. (A.6), and yields

$$p_m = [s(N_f - \eta_f) F(-2m, -\eta_f', 2\gamma_f + 1, y)$$

$$- t\eta_f' F(-2m, -\eta_f' + 1, 2\gamma_f + 1, y)] v^{2m}$$

$$q_m = [s(N_f - \eta_f) F(-2m-1, -\eta_f', 2\gamma_f + 1, y)$$

$$- t\eta_f' F(-2m-1, -\eta_f' + 1, 2\gamma_f + 1, y)] v^{2m+1}$$

$$s = \sqrt{1+\gamma_i}\sqrt{1+\theta_f} + \sqrt{1-\gamma_i}\sqrt{1-\theta_f}$$

$$t = \sqrt{1+\gamma_i}\sqrt{1+\theta_f} - \sqrt{1-\gamma_i}\sqrt{1-\theta_f}$$

$$y = \frac{2}{1+N_f}$$

$$v = 1 + \frac{1}{N_f},$$

which is Eq. (12) in Ref. 25. The integral over the discrete states needs be made, since the observed binding energy is

less than the hydrogenic binding energy. This approximation is also made by Merzbacher[21] in evaluating Eq. (2.27).

Jamnik and Zupančič evaluated Eq. (A.1) for $E_1/\lambda u_K$ less than 0.01, where E_1 is the proton energy, λ is the ratio of the proton to electron mass, and u_K is the observed K-shell ionization energy. They found the relativistic PWBA to lie above the PWBA by as much as a factor of three. The author has attempted to repeat this calculation for $E_1/\lambda u_K \sim 0.05$ and has found the integral over E_f of Eq. (A.1) to diverge. Chang, Morgan, and Blatt[94] report the same difficulty. The calculation proceeded by expanding the hypergeometric functions in the variable y (see Eq. (2.1.4) of Ref. 92 for the form of the expansion) in Eq. (A.16) in a polynomial. Terms through m = 2 were kept. The sum over final states went to $\eta_f = \pm 15$. The integral over E_f was done using the composite Simpson's rule.[95]

One is drawn to the conclusion that the attempt to apply Eq. (A.15) to the region of moderate momentum transfers introduces the divergence. An alternate method of calculation would be to integrate Eq. (A.12) numerically. The integral would be the product of a Bessel function, powers of r, an exponential in r, and a confluent hypergeometric function. I have not attempted this approach; however, the method might prove fruitful.

Attempts to evaluate expressions involving hypergeometric functions over wide ranges of their arguments usually meet with great difficulties. However, in the case of inner-

shell ionization by heavy ions, an attempt would be justified. We have seen in this dissertation that experimental data is now reliably measurable to ±8 per cent and is self-consistent to within ±2 per cent. Disparities between theory and experiment, however, are as high as a factor of two. If agreement between experiment and theory can be brought to within the ±8 per cent experimental errors, the quality of the existing data could be evaluated in a consistent way. One could thus enhance the technological applicability of the ionization process. We have noted in Chap. IV that the theoretical development that most nearly describes the data would be the PWBAR with Coulomb deflection, binding energy, and projectile velocity corrections. I conclude that studies pursuant of extending this theory are needed.

Table I

Target Thickness

Element	Chemical Composition	Thickness ($\mu g/cm^2$)
Se	metal	12.4±0.03
Br	Na Br	17.4±0.04
Rb	$Rb_2 O_3$	11.1±0.03
Sr	$Sr(NO_3)$	1.92±0.06
Y	metal	8.81±0.22
Mo	$Mo O_3$	35.6±0.09
Pd	metal	44.1±0.11

Table II

Fluorescence Yields

Element	ω_K (Calculated[a])	ω_K (Experimental[b])
Se	0.602	0.596±0.032
Br	0.629	0.622±0.032
Rb	0.679	0.669±0.008
Sr	0.702	0.702±0.026
Y	0.722	0.711±0.031
Mo	0.776	0.764±0.032
Pd	0.833	0.819±0.030

[a]From Ref. 85. These values used in this work.

[b]From Ref. 60.

Table III

X-Ray and Ionization Cross Sections for Proton Bombardment

Energy (MeV)	$\sigma_{x\text{-ray}}$ (barns)	σ_I this work (barns)	$\sigma_{I\ CBEA}$[a] (barns)	$\sigma_{I\ BEA}$ (barns)	$\sigma_{I\ PWBA}$ (barns)	$\sigma_{I\ PWBAC}$[b] (barns)	σ_I previous work (barns)
Element Se							
2.000	11.5	19.1 ±1.5	24.0	19.6	27.0	20.3	18.8[d]
1.800	8.57	14.2 ±1.1	18.5	14.8	21.0	15.4	
1.600	6.54	10.9 ±0.9	13.7	10.7	15.6	11.3	
1.400	4.41	7.32 ±0.59	9.60	7.33	11.0	7.74	
1.200	2.81	4.67 ±0.37	6.24	4.64	7.21	4.86	
1.000	1.86	3.09 ±0.25	3.63	2.65	4.28	2.72	2.20[d]
0.800	0.849	1.41 ±0.12	1.79	1.30	2.20	1.29	
0.600	0.291	0.484±0.040	0.630	0.507	0.881	0.456	
0.400	0.0716	0.119±0.015	0.0775	0.131	0.208	0.0924	
Element Br							
2.000	10.4	16.6 ±1.3	18.2	14.6	20.3	15.3	
1.800	8.31	13.2 ±1.1	14.0	11.0	15.7	11.7	
1.600	6.03	9.58 ±0.78	10.3	7.90	11.7	8.39	
1.400	4.47	7.10 ±0.56	7.15	5.36	8.15	5.70	
1.200	2.71	4.32 ±0.34	4.61	3.38	5.29	3.57	
1.000	1.56	2.48 ±0.20	2.66	1.93	3.11	1.97	
0.800	0.793	1.26 ±0.10	1.29	0.948	1.58	0.913	
0.600	0.334	0.532±0.045	0.435	0.369	0.627	0.325	

Table III cont.

Energy (MeV)	$\sigma_{x\text{-ray}}$ (barns)	σ_I this work (barns)	$\sigma_{I\ CBEA}$[a] (barns)	$\sigma_{I\ BEA}$ (barns)	$\sigma_{I\ PWBA}$ (barns)	$\sigma_{I\ PWBAC}$[b] (barns)	σ_I previous work (barns)
Element Rb							
2.000	5.43	8.11 ±0.50	10.6	8.27	11.8	8.89	9.8[e]
1.800	4.47	6.68 ±0.41	8.06	6.15	9.02	6.60	
1.600	3.62	5.42 ±0.34	5.86	4.38	6.58	4.70	
1.400	2.37	3.54 ±0.23	4.02	2.95	4.54	3.13	
1.200	1.32	1.97 ±0.15	2.55	1.84	2.91	1.91	
1.000	0.927	1.39 ±0.10	1.44	1.04	1.68	1.05	0.87[c] 1.13[e]
0.800	0.408	0.609 ±0.041	0.671	0.505	0.828	0.467	
0.600	0.124	0.186 ±0.016	0.206	0.191	0.318	0.160	
0.400	0.0277	0.0414±0.0055		0.0445	0.0758	0.0291	
Element Sr							
2.000	5.28	7.36 ±0.57	8.16	6.27	9.07	6.75	
1.800	3.94	5.50 ±0.43	6.16	4.65	6.88	5.01	
1.600	2.69	3.75 ±0.29	4.46	3.29	4.97	3.53	
1.400	1.81	2.52 ±0.20	3.04	2.21	3.40	2.35	
1.200	1.18	1.65 ±0.12	1.91	1.37	2.16	1.41	
1.000	0.702	0.980±0.073	1.07	0.770	1.24	0.764	
0.800	0.364	0.510±0.039	0.487	0.370	0.614	0.338	
0.600	0.0797	0.110±0.009	0.141	0.138	0.234	0.114	

Table III cont.

Energy	$\sigma_{x\text{-ray}}$ (barns)	σ_I this work (barns)	σ_I CBEA[a] (barns)	σ_I BEA (barns)	σ_I PWBA (barns)	σ_I PWBAC[b] (barns)	σ_I previous work (barns)
Element Y							
2.000	3.94	5.45 ±0.41	6.30	4.78	6.96	5.16	
1.800	3.09	4.27 ±0.32	4.74	3.53	5.24	3.81	
1.600	2.11	2.92 ±0.22	3.41	2.49	3.78	2.66	
1.400	1.43	1.98 ±0.15	2.31	1.66	2.57	1.75	
1.200	0.881	1.22 ±0.09	1.45	1.03	1.62	1.05	
1.000	0.480	0.666 ±0.049	0.798	0.573	0.919	0.557	
0.800	0.220	0.304 ±0.022	0.354	0.272	0.448	0.248	
0.600	0.0720	0.0994±0.0073	0.0953	0.100	0.170	0.0815	
Element Mo							
2.000	2.05	2.65 ±0.21	2.99	2.18	3.22	2.36	
1.800	1.48	1.91 ±0.14	2.22	1.59	2.39	1.71	
1.600	1.13	1.46 ±0.10	1.57	1.11	1.69	1.17	
1.400	0.679	0.876 ±0.064	1.05	0.732	1.13	0.755	
1.200	0.402	0.518 ±0.038	0.641	0.447	0.699	0.444	
1.000	0.218	0.280 ±0.021	0.339	0.245	0.388	0.228	
0.800	0.0968	0.125 ±0.009	0.138	0.115	0.184	0.0996	
0.600	0.0294	0.0379±0.0034	0.0268	0.0415	0.0660	0.0309	
0.400	0.00472	0.00609 ± 0.00105		0.0087	0.0145	0.00491	

Table III cont.

Energy (MeV)	$\sigma_{x\text{-ray}}$ (barns)	σ_I this work (barns)	σ_I CBEA[a] (barns)	σ_I BEA (barns)	σ_I PWBA (barns)	σ_I PWBAC[b] (barns)	σ_I previous work (barns)
Element Pd							
2.000	0.755	0.906 ±0.064	1.18	0.813	1.21	0.873	1.19[e]
1.800	0.541	0.649 ±0.046	0.862	0.586	0.883	0.615	
1.600	0.386	0.463 ±0.032	0.603	0.404	0.614	0.417	
1.400	0.249	0.299 ±0.021	0.391	0.263	0.403	0.295	
1.200	0.152	0.182 ±0.013	0.228	0.158	0.244	0.147	
1.000	0.0714	0.0857±0.0062	0.112	0.0853	0.133	0.0755	
0.800	0.0328	0.0394±0.0028	0.0375	0.0385	0.0613	0.0310	
0.600	0.00812	0.00975 ± 0.00073	0.00233	0.0125	0.0218	0.00879	

[a]From Ref. 24.
[b]From Ref. 22.
[c]From Ref. 26.
[d]From Ref. 27.
[e]From Ref. 28.

Table IV

K_α/K_β Ratios

Element	K_α/K_β This work	K_α/K_β Calculated[a]	K_α/K_β Experimental
Se	6.17±0.56	6.16	
Br	5.90±0.44		
Rb	5.71±0.46	5.62	5.62[b]
Sr	5.02±0.41	5.46	5.95[c] 5.80[d]
Y	5.51±0.47		
Mo	5.10±0.39	5.05	
Pd	6.34±0.57		

[a]From Ref. 86.

[b]From Ref. 49.

[c]From Ref. 50.

[d]From Ref. 51.

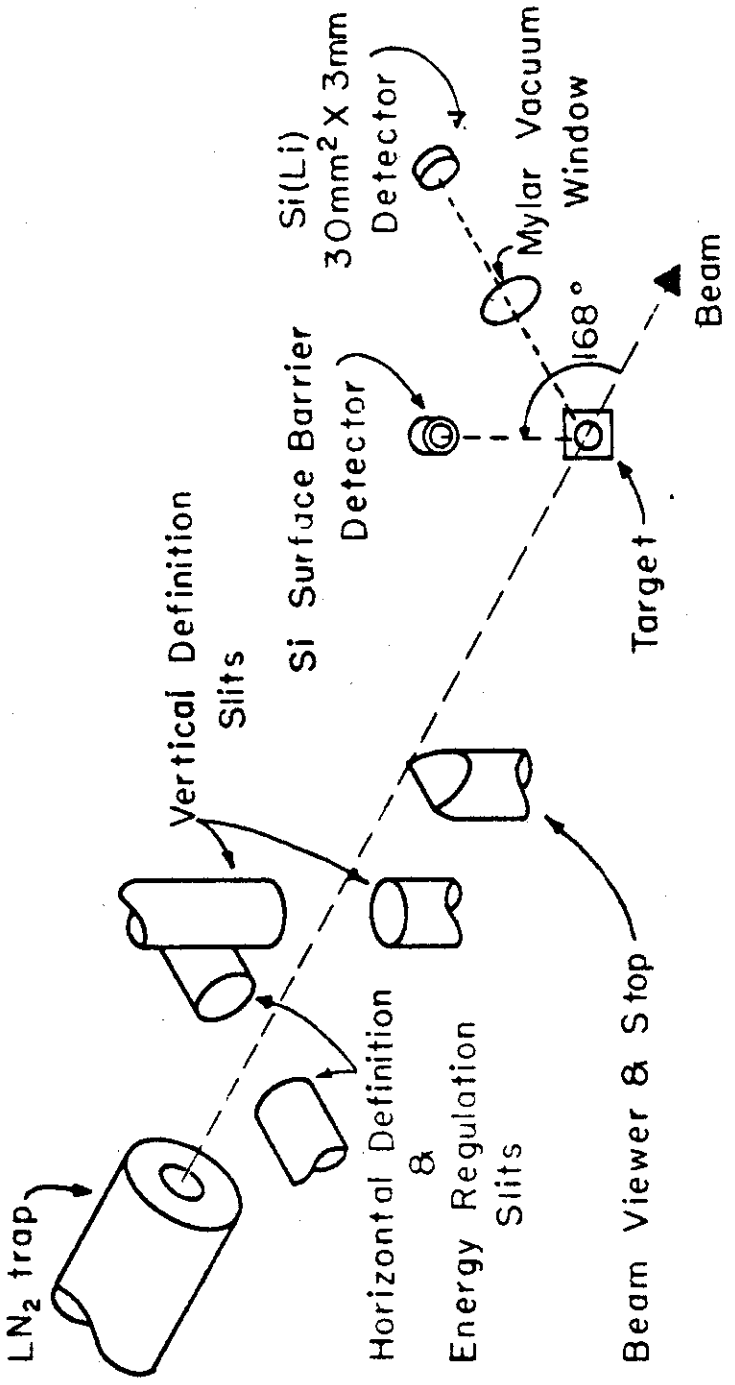

Fig. 1--Experimental station used for ion induced x-ray studies.

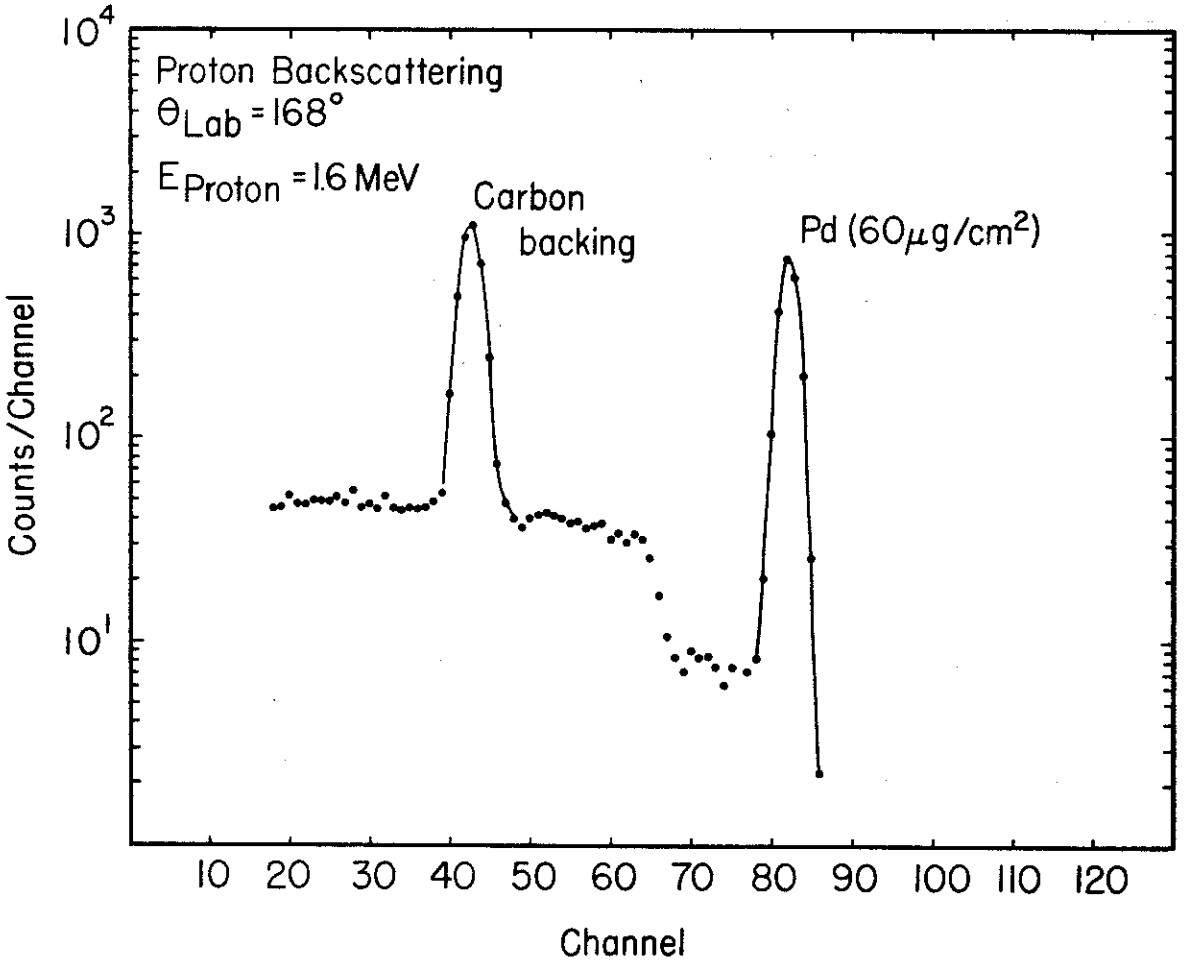

Fig. 2--Typical backscattered proton spectrum from Pd.

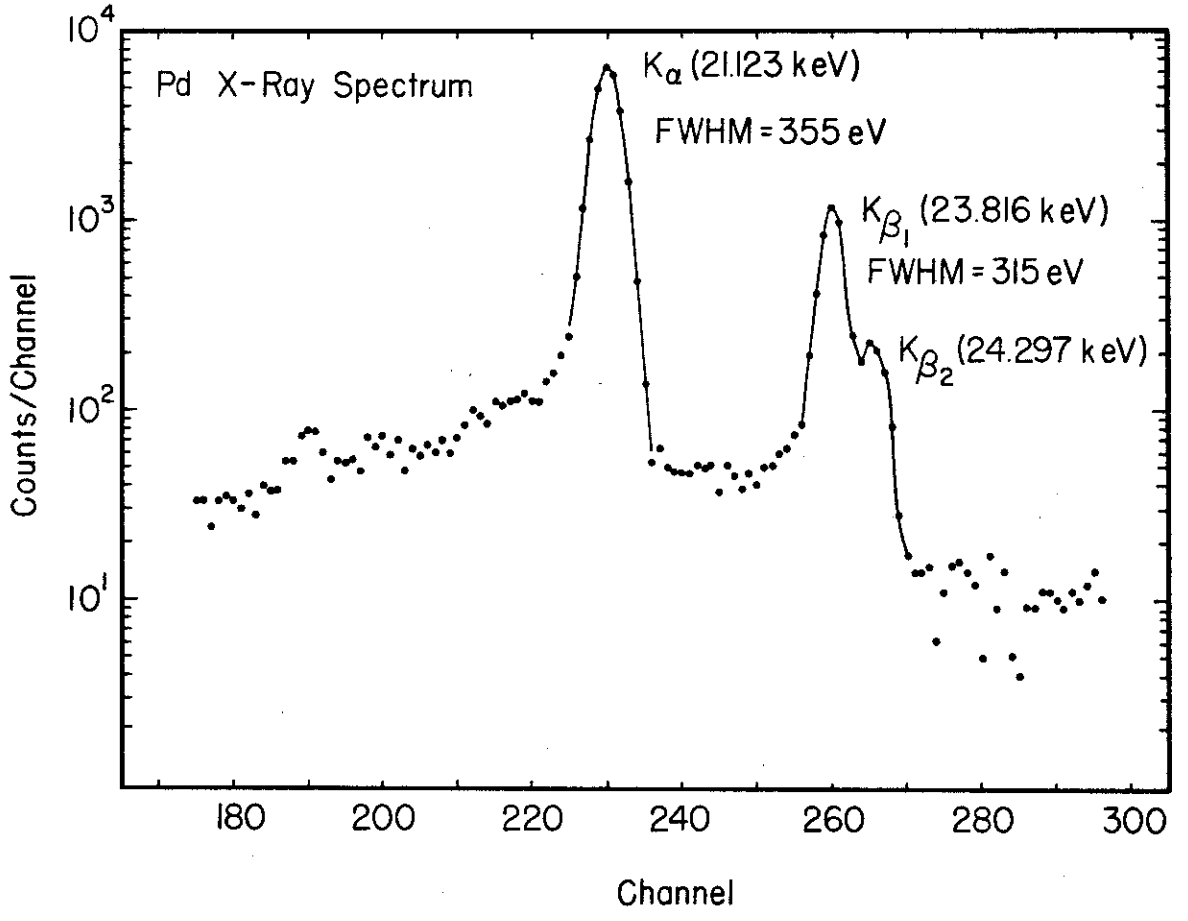

Fig. 3--Typical x-ray spectrum from Pd observed by a 168 eV resolution Si(Li) detector.

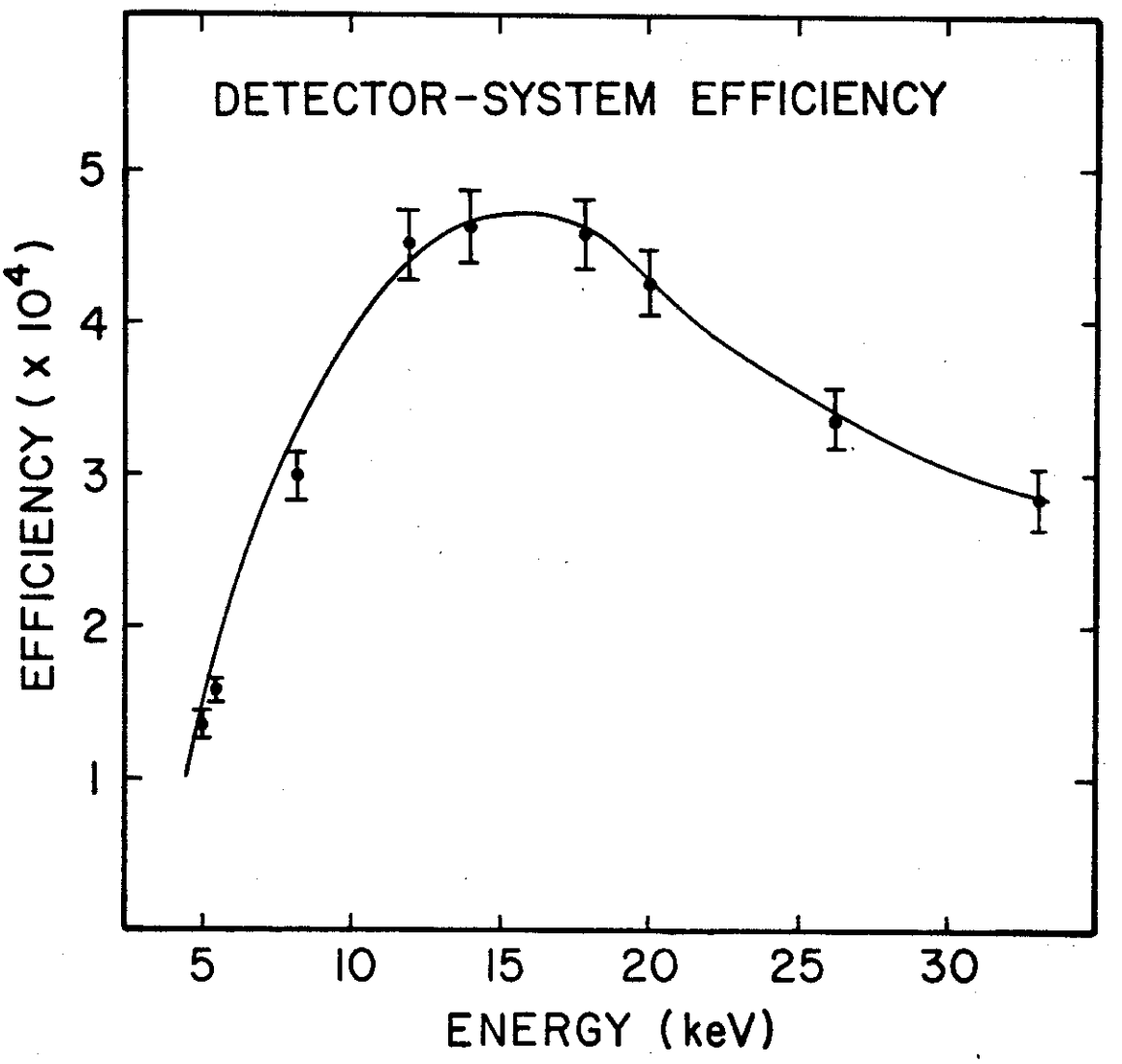

Fig. 4--Absolute detector-system efficiency

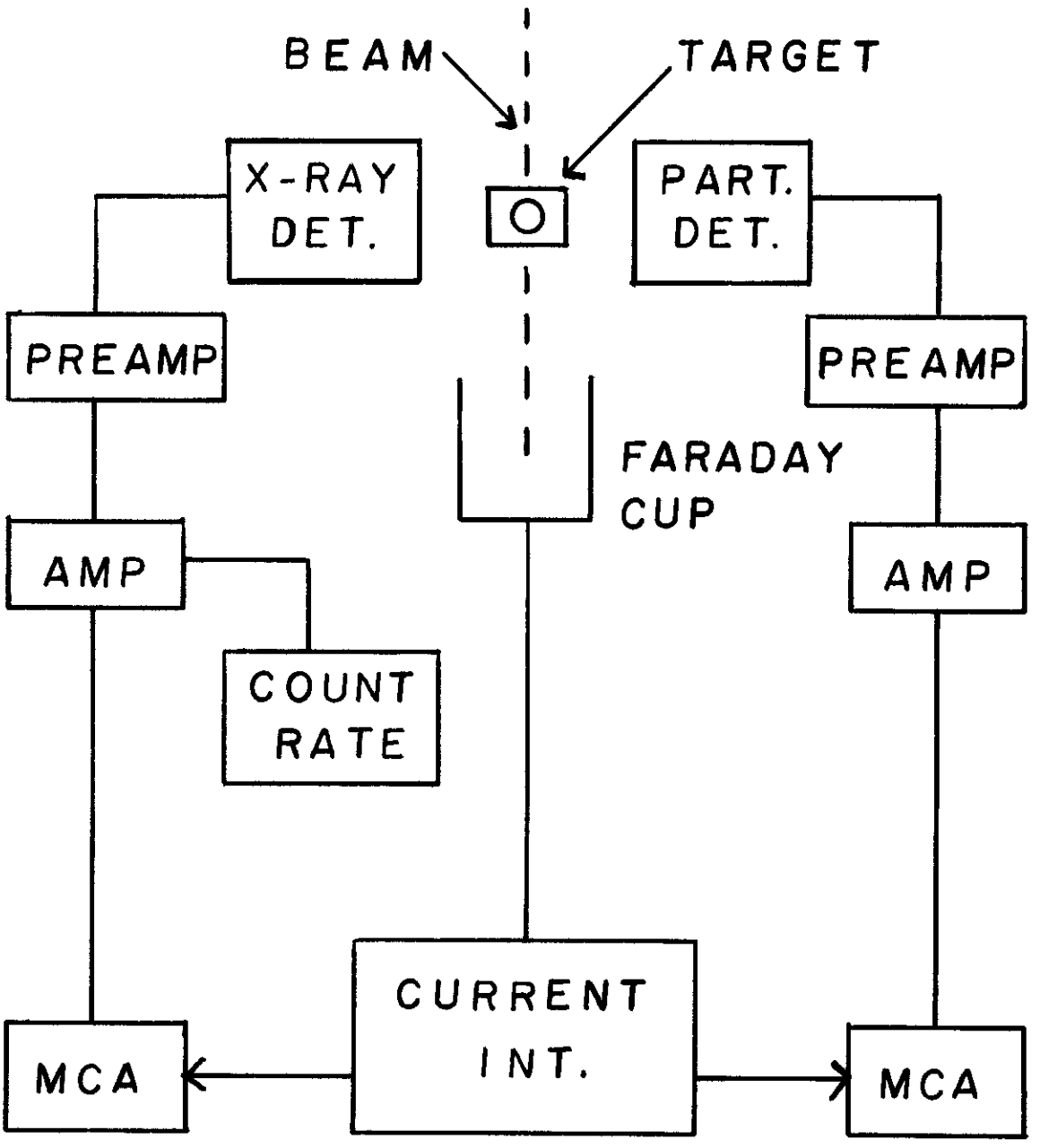

Fig. 5--Electronics block diagram.

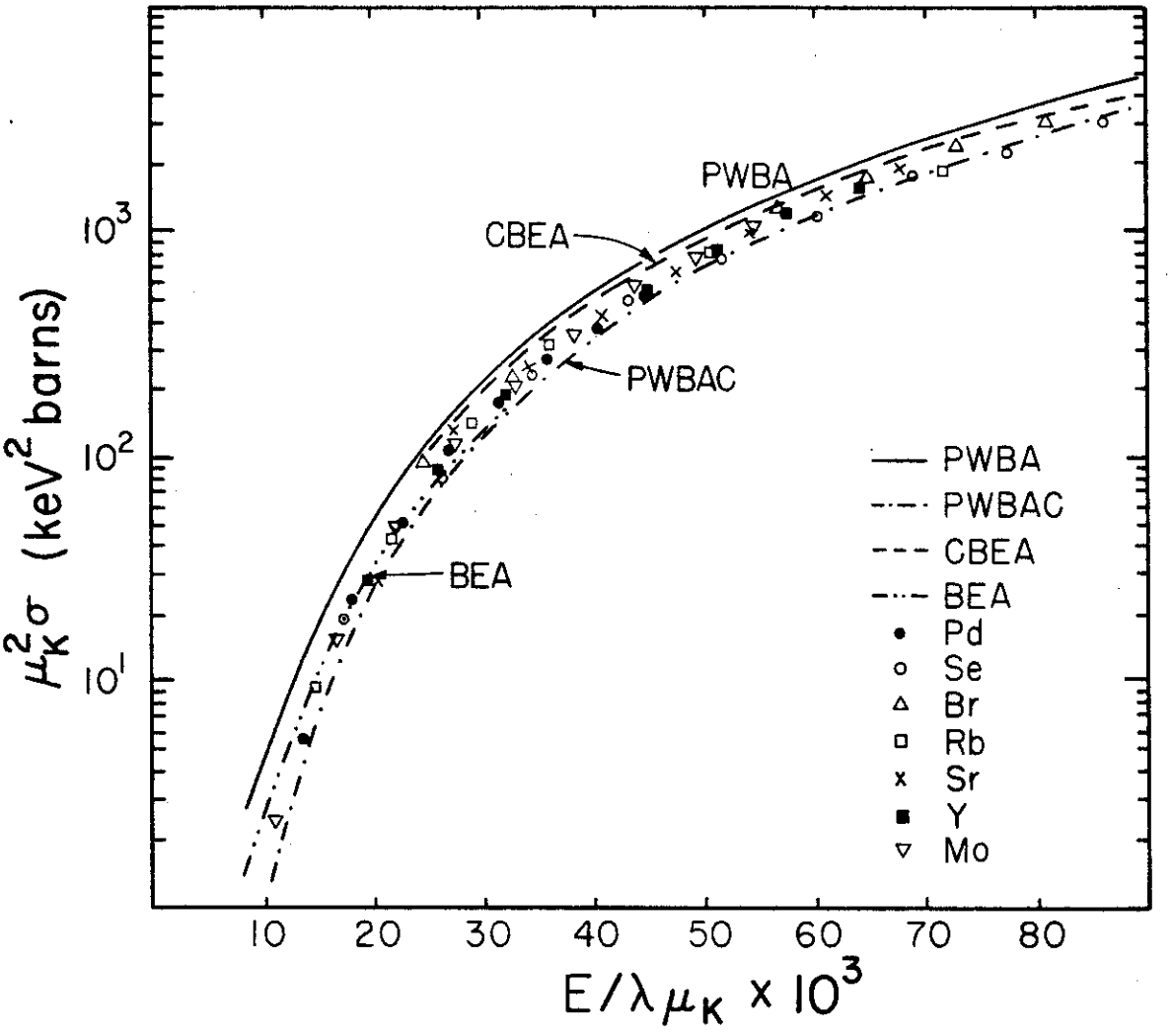

Fig. 6--The measured K-shell ionization cross section for selected elements Se to Pd plotted as a universal curve, where λ is the ratio of the proton mass to the electron mass, and u_K is the K-shell ionization energy. Comparison is made to the PWBA, PWBAC, BEA, and CBEA.

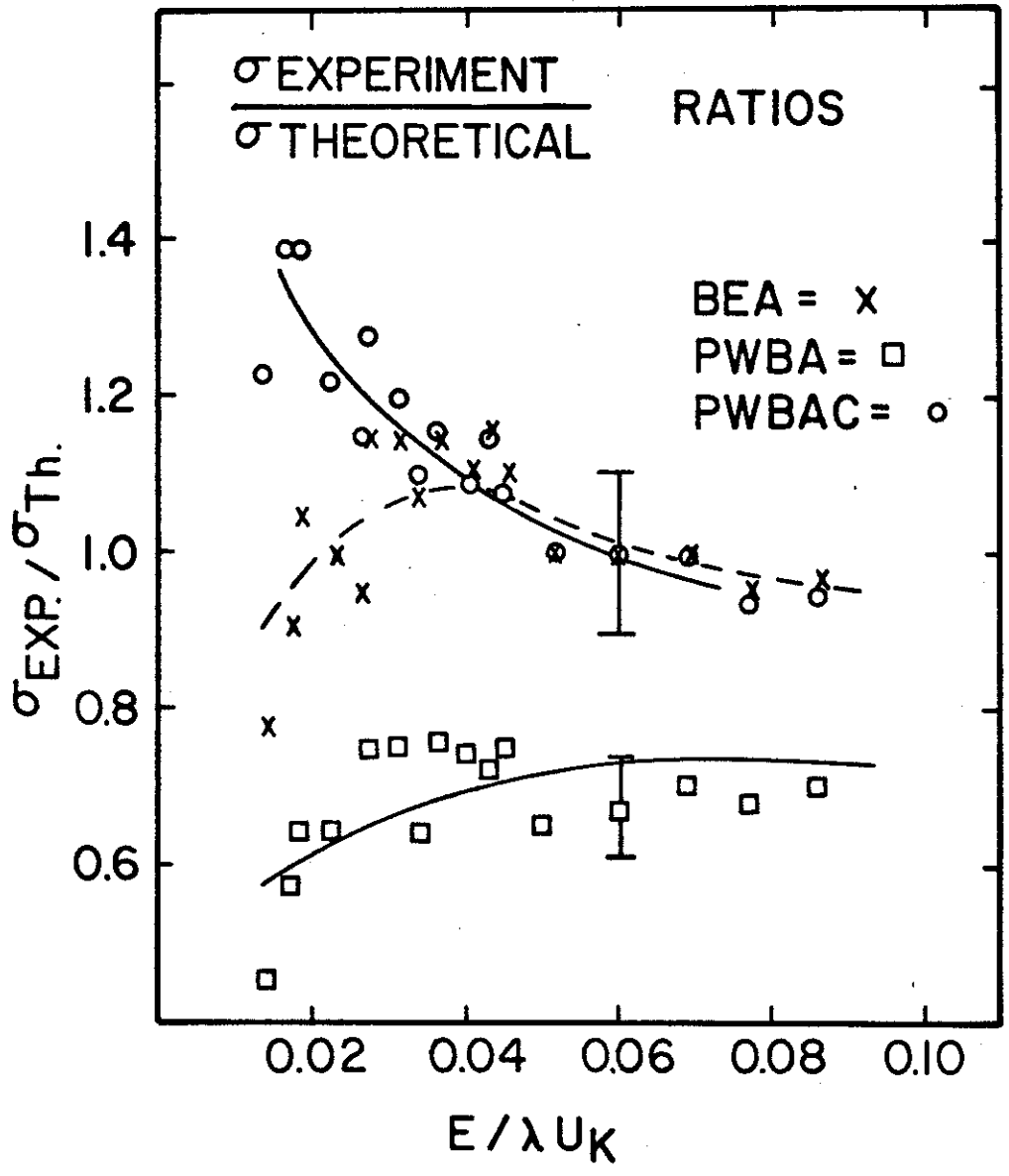

Fig. 7--The ratios of the experimental ionization cross sections to the PWBA, PWBAC, and BEA ionization cross sections for the elements Se and Pd.

REFERENCES

1. E. Elab and M. Nakamura, Nucl. Inst. Methods 41, 161 (1966).

2. T. B. Johansson, R. Akselsson and S. A. E. Johansson, Nucl. Instr. Methods 84, 141 (1970).

3. R. F. Carlton, J. L. Duggan and J. Lin, Bull. Am. Phys. Soc. 17, 89 (1972).

4. T. J. Gray, R. Lear, R. J. Dexter, F. N. Schwettmann, and K. C. Wiemer, Thin Solid Films 19, 103 (1973).

5. J. D. Garcia, R. J. Fortner, and T. M. Kavanagh, Rev. Mod. Phys. 45, 111 (1973).

6. C. H. Rutledge and R. L. Watson, Atomic Data and Nuclear Data Tables 12, 195 (1973).

7. R. Lear and T. J. Gray, Phys. Rev. A 8, 2469 (1973).

8. R. Lear, dissertation (North Texas State University, Denton, Texas, 1973).

9. T. L. Criswell and T. J. Gray, Phys. Rev. A (to be published).

10. T. L. Criswell and Tom J. Gray, Bull. Am. Phys. Soc 18, 558 (1973).

11. N. Khelil and T. J. Gray (submitted to Phys. Rev. A).

12. N. Khelil, dissertation (North Texas State University, Denton, Texas, 1973).

13. F. Abrath and T. J. Gray, Phys. Rev. A 9, 682 (1974).

14. F. Abrath and T. J. Gray, Phys. Rev. A (to be published).

15. F. Abrath, dissertation (North Texas State University, Denton, Texas, 1974).

16. M. Light, thesis (North Texas State University, Denton, Texas, 1973).

17. N. Vora, private communication.

18. T. MacBroom, thesis (North Texas State University, Denton, Texas, 1974).

19. R. Payne, private communication.

20. B. Crosby, thesis (North Texas State University, Denton, Texas, 1973).

21. E. Merzbacher and H. W. Lewis, in Handbuch der Physik, edited by S. Flugge (Springer-Verlang, Berlin, 1958), Vol. 34, p. 166ff.

22. George Basbas, Werner Brandt, and Roman Laubert, Phys. Rev. A7, 983 (1973).

23. J. D. Garcia, E. Gerjouy, and J. E. Welker, Phys. Rev. 165, 66 (1968).

24. J. S. Hansen, Phys. Rev. A8, 8 (1973).

25. D. Jamnik and C. Zupančič, Kgl. Dansk. Vidensk. Selsk., Mat.-Fys. Medd. 31, No. 2. (1957).

26. R. C. Bearse, D. A. Close, J. J. Malanify, and C. J. Umbarger, Phys. Rev. A7, 1269 (1973).

27. J. L. Duggan, R. P. Chaturvedi, C. C. Sachtleben, J. Lin, and R. F. Carlton, private communication.

28. D. V. Ferree, thesis (University of Tennessee, Knoxville, Tennessee, 1972).

29. J. Gray, Proc. Roy. Soc. A 85, 131 (1910).

30. J. Chadwick, Phil. Mag. 24, 594 (1912).

31. J. Chadwick and A. S. Russell, Proc. Roy. Soc. Lond. 88, 217 (1913).

32. J. J. Thomson, Phil. Mag. 28, 620 (1914).

33. F. P. Slater, Phil. Mag. 42, 904 (1921).

34. C. Gerthsen, Z. Physik 36, 540 (1926).

35. W. Bothe and H. Franz, Z. Physik 52, 466 (1929).

36. H. A. Barton, J. Franklin Inst. 209, 1 (1930).

37. C. Gerthsen and W. Reusse, Phys. Z. 34, 478 (1933).

38. O. Peter, Ann. Phys., Lpz. 27, 299 (1936).

39. W. Henneberg, Z. Physik 86, 592 (1933).

40. M. S. Livington, F. Genevese, and E. J. Konopinski, Phys. Rev. 51, 835 (1937).

41. J. M. Cork, Phys. Rev. 59, 957 (1941).

42. J. Urbanec and C. Simane, Czech. J. Phys. 5, 40 (1955).

43. J. W. Lewis, B. E. Simmons, and E. Merzbacher, Phys. Rev. 91, 943 (1953).

44. P. R. Bevington and E. M. Bernstein, Bull. Amer. Phys. Soc. 1, 198 (1956).

45. E. M. Berstein and H. W. Lewis, Phys. Rev. 95, 83 (1954).

46. C. Zupancic and T. Huus, Phys. Rev. 94, 205 (1954).

47. J. M. Hansteen and S. Messelt, Nucl. Phys. 2, 526 (1956).

48. B. Singh, Phys. Rev. 107, 711 (1957).

49. S. Messelt, Nucl. Phys. 5, 435 (1958).

50. R. C. Jopson, J. Mark, and C. D. Swift, Phys. Rev. 127, 1612 (1962).

51. J. M. Khan and D. L. Potter, Phys. Rev. 133, A890 (1964).

52. J. M. Khan, D. L. Potter, and R. D. Worley, Phys. Rev. 134, A316 (1964).

53. J. M. Khan, D. L. Potter, and R. D. Worley, Phys. Rev. 135, A511 (1964).

54. J. M. Khan, D. L. Potter, and R. D. Worley, Phys. Rev. 136, A108 (1964).

55. J. M. Khan, D. L. Potter, and R. D. Worley, Phys. Rev. 139, A1735 (1965).

56. J. M. Khan, D. L. Potter, and R. D. Worley, Phys. Rev. 145, 23 (1966).

57. J. M. Khan, D. L. Potter, R. D. Worley, and H. P. Smith, Phys. Rev. 148, 413 (1966).

58. J. M. Khan, D. L. Potter, R. D. Worley, and H. P. Smith, Phys. Rev. 163, 81 (1967).

59. The values for Ag were extrapolated from the Pb values.

60. W. Bambynek, B. Crasemann, R. W. Fink, H. U. Freund, H. Mark, C. D. Swift, R. E. Price, and P. Venugopala Rao, Rev. Mod. Phys. 44, 716 (1972).

61. P. Richard, M. Senglaub, B. Johnson, and C. F. Moore, Appl. Phys. Lett. 21, 13 (1972).

62. F. P. Larkins, J. Phys. B4, L29 (1971).

63. P. Richard, I. L. Morgan, T. Furuta, and D. Burch, Phys. Rev. Letters 23, 1009 (1969).

64. J. Lin, J. L. Duggan, and R. F. Carlton, "Proceedings of the International Conference on Inner-Shell Ionization Phenomena and Future Applications," April 1972, Atlanta, Georgia, edited by R. W. Fink, S. T. Manson, J. M. Palms, and P. V. Rao (USAEC Report No. CONF-720404, Oak Ridge, Tenn., 1973), P. 998.

65. J. Bang and J. M. Hansteen, Kgl. Dansk. Vidensk. Selsk., Mat-Fys. Medd. 31, No. 13 (1959).

66. M. Gryzinaki, Phys. Rev. 138, A305 (1965).

67. N. F. Mott and S. N. Massey, The Theory of Atomic Collisions, 3rd. ed. (Oxford Univeristy Press, London, 1965), pp. 327-331.

68. N. F. Mott, Proc. Camb. Phil. Soc 27, 553 (1931).

69. L. I. Schiff, Quantum Mechanics, 3rd. ed. (McGraw-Hill Book Company, New York, 1968), p. 318.

70. G. Arfken, Mathematical Methods for Physicists, 2nd. ed. (Academic Press, New York, 1970), Chap. 8.6.

71. J. C. Slater, Phys. Rev. 36, 57 (1930).

72. G. S. Khandelwal, B.-H. Choi, and E. Merzbacher, At. Data 1, 103 (1969).

73. E. Gerjouy, Phys. Rev. 148, 55 (1966).

74. J. D. Garcia, Phys. Rev. A 1, 280 (1960).

75. M. E. Rose and R. K. Osborn, Phys. Rev. 93, 1315 (1954).

76. M. E. Rose, Phys. Rev. 51, 484 (1937).

77. P. A. M. Dirac, The Principles of Quantum Mechanics, 4th. ed. (Oxford University Press, London, 1958), p. 257.

78. M. L. Roush, L. A. West, and J. B. Marion, Nucl. Phys. A147, 235 (1970).

79. P. B. Lyons, J. W. Toeys, D. G. Sargood, Nucl. Phys. A130, 1 (1969).

80. E. Storm and H. I. Israel, Nucl. Data A 7, 565 (1970).

81. R. D. Evans, The Atomic Nucleus, (McGraw-Hill Book Company, New York, 1955), p. 711.

82. R. J. Gehrke and R. A. Rokken, Nucl. Inst. Methods 97, 219 (1971).

83. J. S. Hansen, J. C. McGeorge, D. Nix, W. D. Schmidt-Ott, I. Unus, and R. W. Fink, Nucl. Instrum. Meth. 106, 365 (1973).

84. Sloan Materials Division, Handbook of Thin Film Materials, (535 East Montecito Street, Santa Barbara, California).

85. V. D. Kostroun, M. H. Chen, and B. Crasemann, Phys. Rev. A 3, 533 (1971).

86. J. H. Scofield, Phys. Rev. A 9, 1041 (1974).

87. D. A. Close, R. C. Bearse, J. J. Malanify, and C. J. Umbarger, Phys. Rev. A 8, 1873 (1973).

88. J. S. Hansen, H. U. Freund, and R. W. Fink, Nucl. Phys. A142, 604 (1970).

89. P. V. Rao, M. H. Chen, and B. Crasemann, Phys. Rev. A 5, 997 (1972).

90. M. E. Rose, Relativistic Electron Theory (John Wiley and Sons, Inc., New York, 1961) p. 25.

91. H. P. Bethe, Ann. d. Physik 4, 443 (1930).

92. A. Erdelyi, W. Magnus, F. Oberhettinger, and F. G. Tricomi, Higher Transcendental Functions I. Bateman Manuscript Project, (McGraw-Hill Book Company, Inc., 1953).

93. A. Erdelyi, Proc. Roy. Soc. Edinb. A 62, 378 (1946-47).

94. C. N. Chang, J. F. Morgan, and S. L. Blatt, private communication.

95. B. Carnahan, H. A. Luther, and J. O. Wilkes, Applied Numerical Methods (John Wiley and Sons, Inc., New York, 1969), p. 77.